Carcass locations implicate cyanobacterial toxicity in a mass elephant mortality event in Botswana

Lomeo, D.[1]*, Tebbs, E.J.[1], Babayani N.D. [2], Chadwick, M.A.[1], Gondwe, M.[2], Jungblut, A.D. [3], McCulloch, G.P[4], Morgan, E.R.[5], Schillereff, D.N.[1], Simis, S.G.H.[6], Songhurst, A.C[4]

[1]King's College London, London, United Kingdom
*Lomeo, D. - davide.lomeo@kcl.ac.uk - twitter: @davidelomeo

Tebbs, E.J. - emma.tebbs@kcl.ac.uk

Chadwick, M.A. - michael.chadwick@kcl.ac.uk

Schillereff, D.N. - daniel.schillereff@kcl.ac.uk

[2]Okavango Research Institute, University of Botswana, Maun, Botswana
Babayani N.D. - NBabayani@ub.ac.bw

Gondwe, M. - mgondwe@UB.AC.BW

[3]Natural History Museum, London, United Kingdom
Jungblut, A.D. - a.jungblut@nhm.ac.uk

[4]Ecoexist, Maun, Botswana
McCulloch, G.P. - gmc.ocb@gmail.com
Songhurst, A.C. - fielddirector@ecoexistproject.org

[5]Queen's University, Belfast, United Kingdom
Morgan, E.R. - Eric.Morgan@qub.ac.uk

[6]Plymouth Marine Laboratory, Plymouth, United Kingdom
Simis, S.G.H. - stsi@pml.ac.uk

*Corresponding Author

This manuscript will be submitted for publication in *Nature Communications* and has not yet been peer reviewed. If accepted, the final version of this manuscript will be available via the "Peer-reviewed Publication DOI' link on this webpage. Please feel free to contact the corresponding author davide.lomeo@kcl.ac.uk; we welcome feedback.

Abstract

The 2020 mass mortality of 350 African elephants (*Loxodonta africana*) in Botswana sparked global concern. These deaths have been linked to cyanobacterial toxins (cyanotoxins) in local watering holes (pans), but evidence remains inconclusive. Our study presents the first detailed spatial analysis that explores the relationship between the ecohydrology of 3,389 regional pans with the locations of deceased elephants. Our findings reveal a significant difference in the distribution of fresh versus older elephant carcasses ($p < 0.001$), suggesting that the die-off event deviates from typical regional patterns of elephant deaths. We identified twenty pans near the sites of fresh carcasses that experienced more phytoplankton (microalgae or cyanobacteria) bloom events in 2020 ($n = 123$) compared to the previous 3 years combined ($n = 23$), exhibiting the highest average phytoplankton biomass of the period 2015-2023 (Normalised Difference Chlorophyll Index > 0.2; $p < 0.001$). These findings suggest a high risk and likelihood of cyanotoxins as the poisoning source. Our spatial analysis indicates elephants walked an average of 16.5 km (± 6.2 km) and died within 88 hours (± 33 hours) from initial exposure, offering metrics that were previously unknown for elephants. This study presents important new evidence that implicates cyanobacterial toxicity in the 2020 mass die-off and provides a general framework for investigation of future mortality events of large mammals. We underscore the need to integrate spatial analysis and ecohydrological assessments to better monitor and mitigate animal mortality events and inform conservation strategies.

Introduction

The 2020 die-off of 350 elephants in Botswana was one of the biggest mortality events of large mammals in southern Africa in recent years. The remote location in the north-eastern sector of Botswana known as the eastern Okavango Panhandle, and timing at the peak of the COVID-19 pandemic, hindered attempts to respond to and investigate the event[1]. Although this area is a known poaching hotspot in Botswana[2], this was ruled out since elephant carcasses were found with tusks intact[3]. Other initial theories included virulent and bacterial causes, such as encephalomyocarditis virus or anthrax, but evidence from the field, such as the fact that only elephants appeared to be affected, the age of dead elephants, and the absence of clinical signs, deemed both unlikely[4]. The cause of the die-off has been officially attributed to environmental intoxication by cyanobacterial toxins, also known as cyanotoxins[5]. A recent study, however, found evidence of *Pasteurella* sp. from carcasses from a die-off event of 35 elephants in neighbouring Zimbabwe in 2020, and suggested this bacterium as an alternative cause of the die-off in Botswana[6].

Cyanobacteria are a group of benthic or planktonic phototrophic prokaryotes often abundant in turbid, stagnant, and nutrient-rich waters, and several bloom-forming species can cause harm due to the production of toxins[7]. Evidence suggests that phytoplankton (microalgae or cyanobacteria) blooms, events in which population size increases exponentially due to favourable conditions[8], are becoming more frequent worldwide due to increased anthropogenic nutrient input and climate change[9]. Links between harmful blooms and animal mortality events are well represented in literature, including cyanotoxin poisoning[10,11]. Cyanobacteria are a common occurrence in water bodies in southern Africa[12,13], and have previously been linked to wildlife mortality events[14].

The Okavango Delta is hydrologically complex and characterised by ephemeral waterbodies filled by seasonal flooding or local rainfall alongside the river itself and associated lakes. Building upon recent studies that revealed increased phytoplankton bloom occurrences in perennial lakes of the Okavango Delta in 2020[15], our research focuses on the eastern Okavango Panhandle area, directly where the die-off occurred. Satellite-derived indices like the Normalised Difference Chlorophyll Index (NDCI)[16] and the Automated Water Extraction Index (AWEI)[17] are used as proxies for phytoplankton biomass and water availability in waterholes or pans. The generic NDCI is used to estimate chlorophyll-a concentration because other diagnostic alternatives do not exist for small and shallow waterbodies. Spatial analysis including reconstruction of animal movement were subsequently used to explore relationships between potential sources of cyanotoxins and specific elephant mortality locations. This is the first demonstration of a comprehensive spatial analysis into large animal mortality, addressing a crucial gap in understanding the relationship between pan conditions and elephant deaths. We investigate whether the proximity of carcasses to pans with suspected phytoplankton bloom activity corroborates the hypothesis that deteriorating water quality has caused the die-off. Our results contribute to elucidating the causes behind such mass mortality events and demonstrate the utility of incorporating spatial analysis into routine wildlife health monitoring. This approach enhances wildlife conservation efforts and informs public health strategies, providing vital insights for potentially preventing and controlling future incidents.

Results

Spatial analysis of elephant carcasses and live elephants

The mass mortality event in Botswana occurred in the eastern Okavango Panhandle region within the concession areas NG11, NG12, and NG13, in the north-easternmost sector of the Okavango Delta (Fig. 1). The area is enclosed by veterinary fences to the north (a double border fence with Namibia) and a 'buffalo fence' to the east and south.

These fences were originally installed to prevent the transmission of infectious diseases from wild animals to domestic animals, like the foot and mouth disease carried by buffalos[18], and lung disease in cattle[19]. An aerial survey carried out in mid-July 2020 to investigate the event using a small aircraft[20] revealed 161 fresh carcasses (estimated from their state of decomposition to have been dead less than 6 months; named carcasses hereafter), 222 old carcasses (dead between 6 months and 10 years; bones hereafter), and 2,682 live elephants across the area[21]. The dead elephants were of varying age, with tusks intact, and no carcasses of other wildlife or livestock species were observed. We used bones as an indication of what a 'normal' or 'natural distribution of carcasses across the eastern Okavango Panhandle should be, whereas we assumed that carcasses with skin were very recent thus associated with the die-off event.

The spatial distribution of elephant carcasses significantly differed from that of bones and live elephants, with carcasses notably closer to pans (Two-Samples Kolmogorov-Smirnov test, KS test, $p<0.001$). Specifically, live elephants were mainly observed in dry woodlands, particularly in the NG11 and NG13 sectors of the eastern Panhandle, and dispersed across the NG12 area, near the Okavango Delta wetland system and along the "buffalo" veterinary fence (Fig. 2). In contrast, bones were scattered more broadly across the landscape, covering an area of approximately 6,500 km², with notable concentrations near the eastern Panhandle's wetlands. Carcasses, however, were primarily found in a more confined area (~4,350 km²), considerably distant from the wetlands and human settlements. Our analysis revealed significant differences in the proximity of each elephant category to water sources (KS test, $p<0.001$). Carcasses were, on average, located closer to pans (1,635 m ± 2,317 m) compared to bones (4,545 m ± 3,477 m) and live elephants (5,672 m ± 3,814 m). Distinct clustering patterns emerged among the categories. Live elephants exhibited the most pronounced clustering, followed by carcasses, then bones. This variance was statistically significant (KS test, $p<0.001$), highlighting different spatial behaviours and associations. Specifically, bones showed the greatest number of clusters (n=14), indicative of widespread dispersion, followed by live elephants (n=13), and carcasses (n=5), with the average number of individuals per cluster being substantially higher for carcasses (n=29±54) than for bones (n=11±11) or live elephants (n=9±5). Notably, a significant portion of the carcasses were found within a single cluster (n=126), hinting at a common underlying cause for these deaths. Given these results, we decided to focus the remainder of the analysis solely on the location of the fresh carcasses arisen from the die-off.

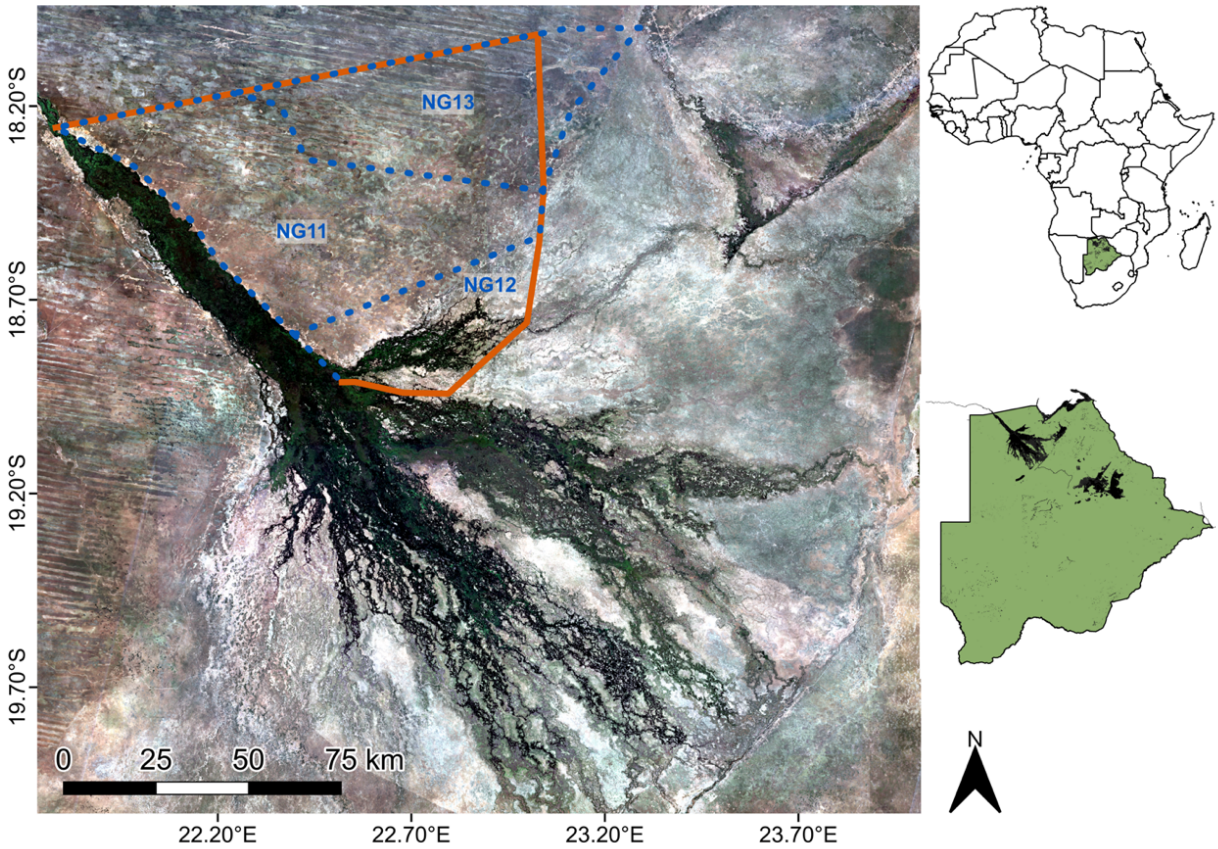

Fig. 1 | Map of the eastern Okavango Panhandle area in northern Botswana and the veterinary fence enclosing it. The satellite image on the left shows the Okavango Delta, located in the north of Botswana, in May 2020. The image was obtained using Google Earth Engine and it is the median product of images captured by Sentinel-2 in the period 15-31/05/2020, at Level-2A (surface reflectance). The blue dotted lines show the boundaries of the concession areas NG11, NG12 and NG13, whereas the orange lines show the boundaries of the veterinary fence, which runs along the border with Namibia in the north. The green shape to the right shows the territory of Botswana, and the black areas within it are areas where water is regularly detected.

Ecohydrology of pans and climate

We identified 3,389 unique pans in the eastern Okavango Panhandle, and examination of their ecohydrology revealed a major shift in water availability and phytoplankton growth between 2019 and 2020. This suggests potential implications for water quality, which may have impacted local wildlife. Using imagery from the Sentinel-2A/B Multispectral Instrument (MSI) from August 2015 to September 2023, we observe strong interannual fluctuations in the number of pans. The highest number of pans was observed in 2021 (n = 3,389), while the lowest was recorded in 2016 (n = 724) (not considering 2015, for which image collection started from August). We employed Moran's I local spatial association statistic to identify pans spatially related with the central locations of carcass clusters, rather than with individual positions (Fig. 1 in Supplementary Information 1). This approach assumes that elephants dying within the same cluster would have faced similar environmental influences from nearby water sources. By analysing cluster centres, we were able to narrow our study to a set of 1,232 pans spatially related to carcasses cluster centres. We conducted a temporal analysis on these pans to assess changes in Normalised Difference Chlorophyll Index (NDCI), used as a proxy for phytoplankton biomass, and Automated Water Extraction Index (AWEI), used as a proxy of water availability, alongside precipitation and temperature data. The data was converted into bi-weekly averages to reduce noise and account for varying satellite overpass (3-5 days), as well as missing images due to cloud cover. NDCI exhibited consistently high values since 2020, contrasting with more variable pre-2020 levels (Fig. 3). AWEI values showed a dramatic increase in water availability from 2020 onwards, diverging from consistently low levels before 2019. Contextualising these findings against background environmental conditions, we found that 2019 had one of the lowest precipitation levels in the period 2012-2022, second only to 2015, and followed by a wet 2020. Temperature in 2019 was much higher than the 2012-2020 average and followed by a relatively cooler 2020. Pans in proximity to carcass cluster centres revealed that a marked increase in water availability coincided with sustained high phytoplankton biomass, as evidenced by post-2019 NDCI. The drastic changes in ecohydrological and climate conditions, particularly in the shift between 2019 (i.e., notably low rainfall and high temperatures) and 2020 (i.e., high rainfall and lower temperature), underscore the likelihood for altered water quality and increased harmful cyanobacteria bloom risks. These environmental dynamics, occurring in tandem with the carcass spatial clustering, provide compelling evidence of water quality deterioration as a significant factor in the mass die-off event.

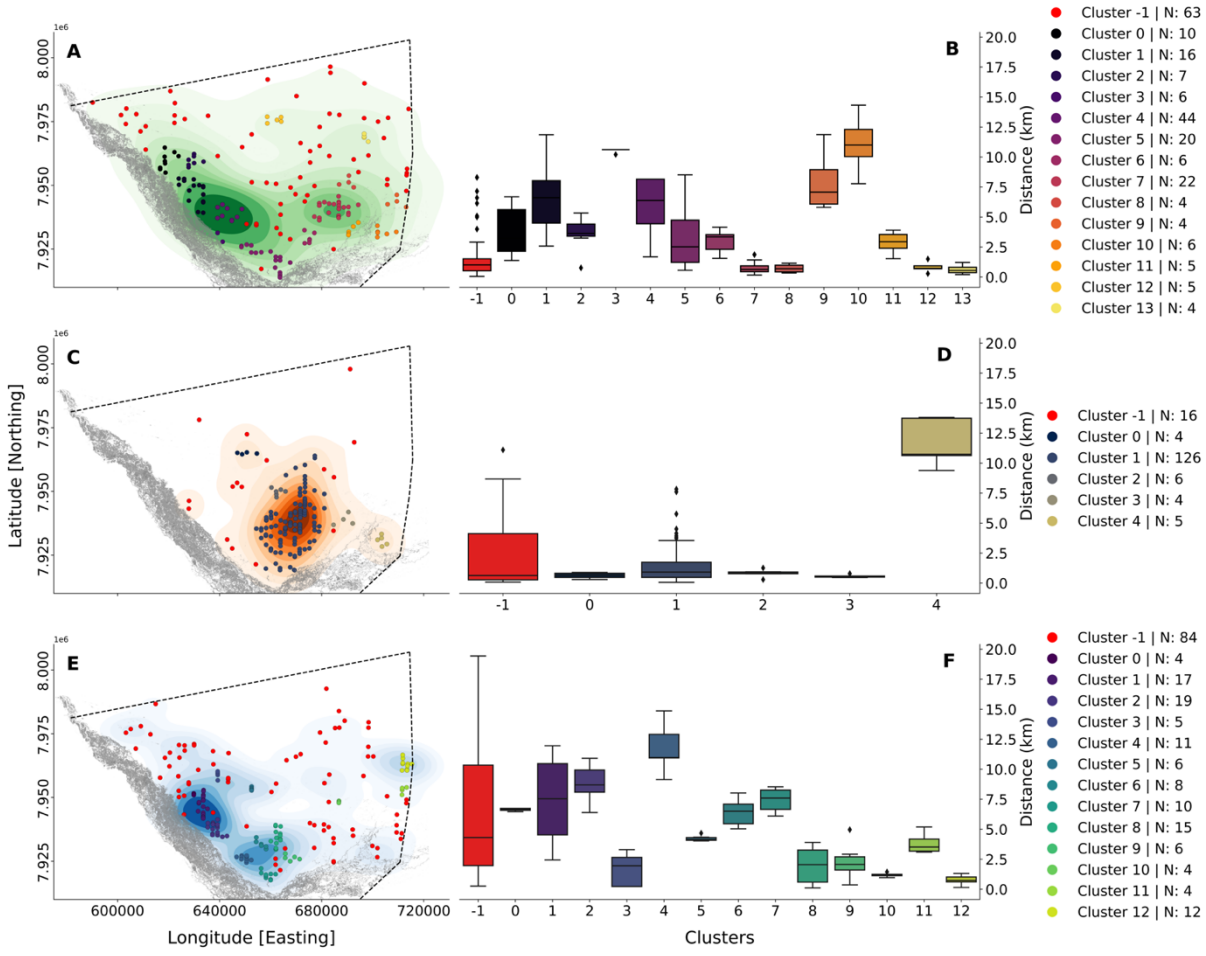

Fig. 2 | Individual clustering of bones, fresh carcasses, and live elephants, kernel density estimates, and related distances to nearest pans. Panels A, C and E show the distribution of bones, fresh carcasses, and live elephants across the eastern Okavango Panhandle, respectively. The coloured shadings around the points represent the kernel density estimates of their distributions, and their colour weight is gradually more intense towards areas of higher concentrations of points. The dotted black lines represent the veterinary fence. Panels B, D and F show boxplots

of the distances between individuals and the nearest pan by cluster for bones, carcasses, and live elephants, respectively. For bones and carcasses, we used the location of pans visible to Sentinel-2 (S2) in April 2020 (i.e., the maximum number of pans detected during the wet season in 2020), whereas for live elephants we used the location of pans visible to S2 at the time of the aerial survey (July 2020). Clusters numbered as -1 and coloured in red in the maps and in the boxplots are groups of individual points that are not statistically significant in the overall dispersion of the three categories ($p>0.05$). These are points that do not belong to any cluster and were not included in the analysis. The points in panels A, C, and E, are coloured such that they match the colour of the cluster they belong to in the boxplots in panels B, D and F, respectively. The legends to the right of the image refer to the panels in the same row, and 'N' refers to the total number of individuals belonging to each of the clusters.

Distance covered by elephants before death

Toxicological timelines of cyanotoxin-related animal deaths in the literature[10] suggest an association between animal size and time of death, the latter occurring between 15 minutes and 120 hours (hrs) after initial exposure (Table 2 in Supplementary Information 1). Most of these studies focus on dogs, cattle, and sheep, with some instances of wildlife reporting like deer and rhinoceros. Extrapolating these findings to elephants, we looked at potential timeframes of 24, 48, 72, 96, 120, and 144 hrs. We then calculated feasible travel ranges using the average speed of 4.5 km per day in this area[22] (Fig. 2 in Supplementary Information 1) to give potential distances between cyanotoxin exposure and death. Furthermore, since the potential distances were calculated concentrically from the cluster centres, we integrated three standard deviation ellipses[23] from cluster centres to account for the directional distribution of the carcasses. This was based on the premise that elephants do not move in a single direction throughout the day[24] and to weigh-in the arrangement of carcasses across the landscape. By considering areas shared by all circular distances and standard deviation ellipses, noting the relatively even spread of carcasses across these areas, we estimated that elephants may have walked an average of 16.5 km (±6.2 km) after initial exposure to harmful cyanobacteria blooms and cyanotoxins and could have died within 88 hrs (±33 hrs).

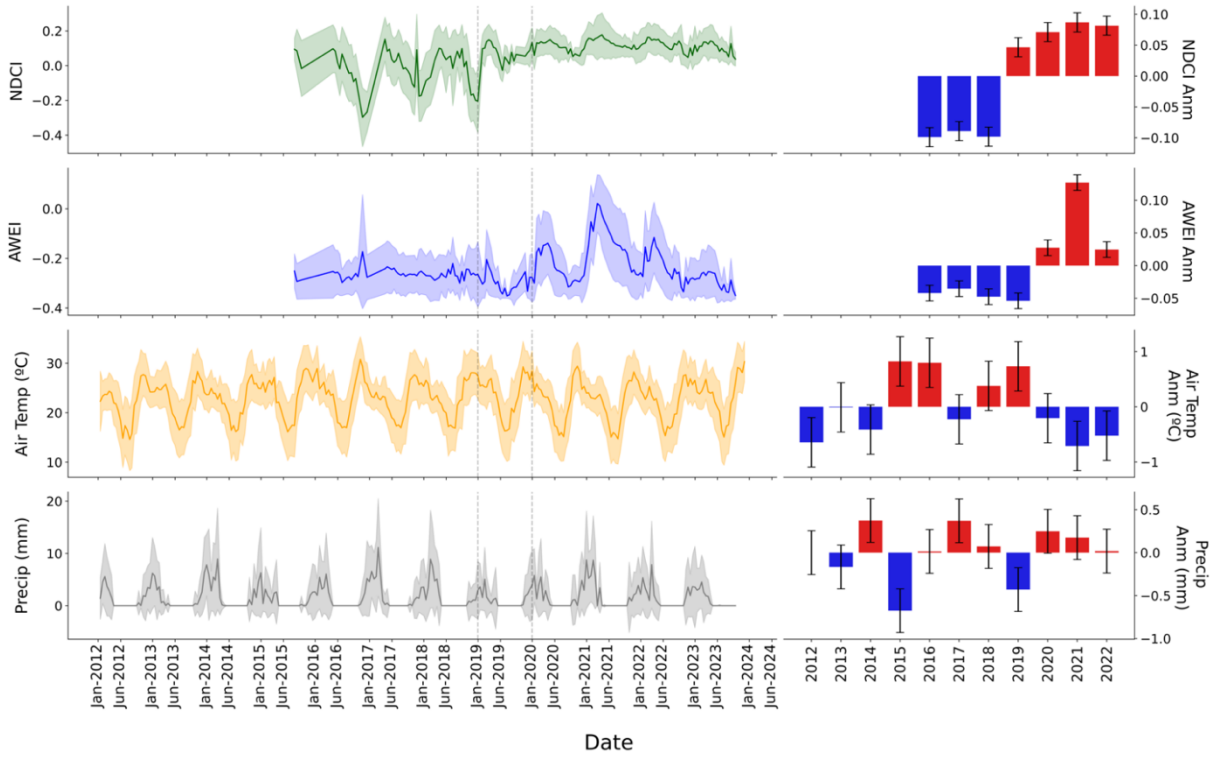

Fig. 3 | Long-term trends in water availability and algal biomass of pans close to fresh elephant carcasses cluster centres. The four panels on the left show the bi-weekly averages of the Normalised Difference Chlorophyll Index (NDCI), the Automated Water Extraction Index (AWEI), air temperature and precipitation, from top to bottom, respectively. The two vertical dotted lines are positioned between January 2019 and January 2020 to highlight the ecohydrological and climatic condition in the Eastern Okavango Panhandle region in the year preceding the mass mortality event. The four bar plots on the right show the anomaly between the annual average and the long term means for NDCI, AWEI, air temperature and precipitation, from top to bottom, respectively. Long-term averages for NDCI and AWEI were limited to the years of Sentinel-2 MSI observations and restricted to the period 2016-2022 to take into account the full 12 months in each year. Long-term averages for air temperature and precipitation were obtained from the period 2010-2022.

Potential sources of the die-off

To indicate high phytoplankton biomass for pans in the region we used a threshold of NDCI = 0.3. We obtained this figure by adding the mean and standard deviation (SD) of NDCI of all previously identified 1,232 pans between Aug 2015 and Sep 2023 for each timestamp (i.e., bi-weekly averages), and pulled the maximum value from the upper SD. Additionally, to identify bloom events we arbitrarily used an increase of NDCI = 0.1 between consecutive timestamps. Using these metrics, we further narrowed the 1,232 pans spatially associated to carcass cluster centres to a set of 151 pans. These pans where within the identified elephants' area of travel, that either showed NDCI > 0.3 or experienced sharp NDCI increases (0.1 units) between consecutive timestamps, or both, at least

once in 2020 (Table 1 in Supplementary Information 2). Strikingly, these 151 pans were all spatially associated with the largest cluster of carcasses (cluster 1; Fig. 2 C and D). These pans showed repeated high-biomass events, with NDCI values up to 0.5, especially in the period 2020 and 2021. The period between April and May 2020 showed the highest algae production, although highly productive pans and bloom events were recorded throughout the year. On average, these pans had water in the period Jan-Jul 2019 only 11% of the time, compared to 55% during the same period in 2020.

To find the most likely sources of poisoning within the elephants' area of travel, we used the same NDCI thresholding described earlier on the 151 pans, specifically looking for pans that experienced repeated (more than twice) high phytoplankton biomass events in 2020, pinpointing 20 pans. Satellite observations revealed that most of the 20 pans were either completely dry prior to 2020, or too small to be detected using MSI images, with a few exceptions (Fig. 4). These pans showed unprecedented phytoplankton biomass between March and May 2020, when elephants were recorded to have died in large numbers. Visual validation of SuperDove images at 3 m spatial resolution confirmed that these pans exhibited repeat blooms between April and May 2020, at different times and intensities (Fig. 3 in Supplementary Information 1). During this period, the size of these 20 pans ranged between 2 and 22 km^2, demonstrating how bloom events occurred irrespective of size or water availability. SuperDove images also revealed that the landscape surrounding these pans was highly heterogeneous, with no obvious links between land cover types around pans and bloom events. Finally, we found that the average distance of these 20 pans from the centre of cluster 1 was 11.6 km (±5.2 km), which aligns with the previously presented estimated distance walked by elephants before dying.

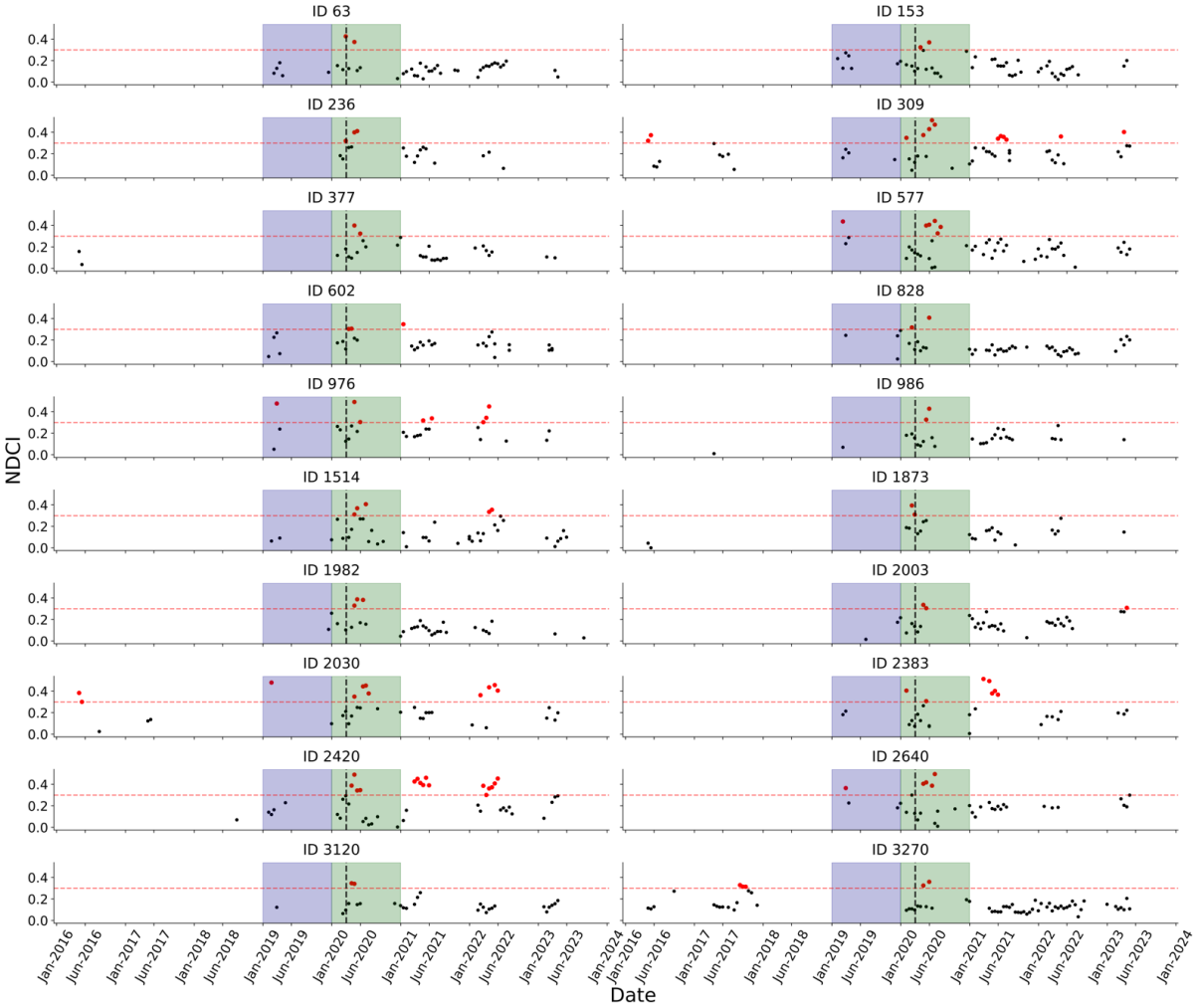

Fig. 4 | NDCI Timeseries of the twenty pans in eastern Okavango Panhandle that showed the highest algal biomass in 2020. Some of the pans show no points prior 2019 because they were likely dry, or too small to be detected using MSI images. Red dots are single observations (pans) when NDCI was >= 0.3. The horizontal red dotted line is placed on NDCI = 0.3 to aid the visualisation, whereas the vertical black dotted line aligns with the time of first elephant death reporting (18/03/2020[25]). Areas shaded in blue and green correspond to the 12 months in 2019 and 2020, respectively.

Discussion

This is the first spatial analysis of the 2020 elephant die-off in the eastern Okavango Panhandle, Botswana. By comparing the locations of carcasses and elephant bones and linking locations to the ecohydrology of the thousands of pans in the study region we provided strong evidence to support the theory that deaths originated from poisoning by cyanotoxins. Our results highlighted that seasonal predominantly rain-fed pans, rather than the permanent waterbodies (i.e., rivers and lagoons) within the panhandle, were the likely source of cyanotoxin exposure. Pans in close proximity to the carcasses showed elevated phytoplankton biomass and repeated bloom events in 2020 compared to previous years, particularly during the period associated with the mass mortality event[1].

Live elephants were mostly found near the Okavango Delta because, in the dry month of July, they move there for water and to forage[26]. Some elephants clustered along the veterinary fence probably because it acts as a physical barrier that prevents them from ranging further[27]. Elephant bones representing deaths in previous years were, in contrast to fresh carcasses, more spread out across the landscape, as demonstrated by the high number of spatial clusters over a wider area (Fig. 2), indicative of a weaker spatial relationship between these points. Some points associated with relatively high numbers of individuals were found nearer the Okavango Delta, but it is challenging to know the cause without relevant data. One likely cause may be mortality from human-elephant conflict, indications of which lie in their proximity to human settlements and the associated increased mortality risk for elephants, owing to high human-elephant competition for shared space and resources in this area of the eastern Okavango panhandle[28]. Heightened competition for space and resources often leads to problem animal control mortalities[29] and sometimes increases the risk of poaching[30]. However, predation and natural causes leading to accumulations of bones cannot be ruled out. Fresh elephant carcasses, on the other hand, were predominantly distributed in a region far from the Okavango River and Delta and human settlements. These carcasses were more densely clustered than bones, indicating that the cause of death was likely localised in this area (Fig. 2). The higher proximity of carcasses to pans compared to bones may be due to the seasonality, since at the time of high elephant mortality in 2020, towards the end of the wet season, elephants tend to stay closer to pans with water[24]. The fact that the average distance between carcasses and the nearest pans was lower than bones (Fig. 2 D) could also be linked to an observed altered behaviour of sick elephants roaming closer to water sources[31,32]. Nonetheless, this spatial pattern is also consistent with water pans as the source of poisoning. The additional spatial and temporal relationships with phytoplankton biomass, such that clustering of fresh carcasses was associated with specific overgrowth events, provides compelling evidence for a causative link, rather than elephants being drawn to water in general, and in contrast to reporting of algal bloom anomalies in the wider region[15]. The strong clustering of carcasses suggests that the event was sudden, with limited dispersal of elephants prior to death. A single cluster of carcasses (cluster 4, Fig. 2 D) was found much further from the others. These elephants may have been part of the same herd, but moved towards this area while sick and their movement was later limited by the standing waters in the Okavango Delta.

Water availability was a major issue in the eastern Okavango Delta in 2019, when it was at its lowest level in the past 8 years (Fig. 3). This was likely driven by lower-than-average precipitation between Oct 2018 and Mar 2019, and higher-than-average temperature in May-Sep 2018. This is particularly relevant for the pans close to the sites of fresh carcasses since these are far from the Okavango Delta and primarily filled by rain or groundwater and are not subject to seasonal flood pulses from the Delta. Lack of precipitation and higher temperatures have to the drying of most pans between 2018 and 2019, and long-standing stagnant waters, where available, likely promoted hyper-eutrophication. Cyanobacteria are frequently abundant in turbid, nutrient-rich waters[7], and tend to dominate these types of water over other phytoplankton species[8]. We theorise that the shift from such a dry 2019 and an extremely wet 2020 may have led to a resuspension of significant amounts of sediments and nutrients, both from the previously dry beds of the pans and the surrounding soil, promoting unprecedented productivity in 2020. The process of nutrients release through sediment resuspension is known[33], and has been documented for the seasonally dry wetlands of the Okavango Delta[34]. Pans that were either completely dry or with little water left in 2019 experienced a dramatic volume of water delivered by rainfall, directly exposing them to sediment resuspension and the associated nutrient release. Nonetheless, it is important to state this process does not affect waterbodies equally, even if very similar in principle, and that the release of nutrients and consequent eutrophication are system dependent[33]. This variability emphasises the need for individual pan analysis in our research, to avoid assuming uniform ecological dynamics across neighbouring pans. Residual cyanotoxins might have persisted in the pans from previous years as shown for deserts' soil crusts[35–37], and there is a possibility that those produced prior to 2020 may have remained in the pans' dried-up bed soil and resuspended in the water. Furthermore, cyanobacteria cells deposited in the sediment from previous year might have inoculated pans' water and increases chances of bloom formation. Unsurprisingly, April and May were the months with the highest frequency of bloom events in 2020. This period is at the end of the rainy season when rainfall is scarce. Full pans with standing water then remain relatively undisturbed and, while temperatures are still high, present ideal conditions for cyanobacterial growth. Our analysis showed that 2015 was also a very dry year (Fig. 3), but the following 2016 rainy season did not deliver the same volumes of water, which may explain why such sustained phytoplankton biomass levels were not observed, and possibly why a mortality event of this size did not occur then.

We estimated that elephants may have walked an average of 16.5 km (±6.2 km) before dying within approximately 88 hrs (±33 hrs). This temporal-spatial dynamic is crucial for understanding the movement patterns of elephants in

response to cyanotoxins exposure and aligns with reported toxicological timelines for other large mammals[10]. It is worth noting that our approach to establish the distance walked by elephants before dying is not based on observed elephant movement, since it is challenging to determine movement behaviours from point analysis, and we are aware that elephants do not move in a single direction throughout the day[22,24]. Therefore, we do not intend to inform on walking behaviours of elephants after initial potential exposure to cyanotoxins. Rather, we attempted to estimate the distance that elephants may have walked before dying, and possibly the time it may have taken them to die after initial cyanotoxin ingestion based on the distribution of the carcasses. These findings could be used to refine future spatial analyses, including assessment of possible sources of cyanotoxin in real-time disease investigations.

By analysing bloom dynamics in the pans spatially associated with carcasses cluster centres, we pinpointed 20 that experienced extremely frequent and severe bloom events of different magnitudes during the critical period between April and May 2020 (Fig. 4). These pans were all spatially associated to cluster 1, the cluster with the largest number of individuals (Fig. 2, D), and were all located an average of 11.6 km from the centre of the cluster. This distance aligns with the estimated distance walked by elephants before dying, making these pans strong candidates as the source of the intoxication. These pans were of various sizes and surrounded by different types of landscapes (Fig. 3 in Supplementary Information 1), so it is challenging, and possibly not realistic, to determine what characteristics of individual pans may make them particularly susceptible to bloom events. Nonetheless, the results show that the bloom trends reported in this study can be extended to smaller pans that we were not able to locate, limited by the 10 m spatial resolution of MSI.

The recent finding of *Pasteurella* spp. in elephant carcasses in Zimbabwe[6] has shed light on the possibility of African elephants to contract the bacterial infection in Botswana also, although it remains uncertain what may have led to its development and transmission[6]. It is possible that elephants in the eastern Okavango Panhandle contracted and spread the disease, leading to the disruption of their immune systems, altered movement, and sensitivity to other mortality factors. Ingestion of higher concentrations, or more potent, cyanotoxins from water compared to 'normal' levels may conversely have led to higher susceptibility to other bacteria, including *Pasteurella* spp., leading to their death. The association between cyanobacterial intoxication and the presence of *Pasteurella multocida*, has previously been reported in a study that found traces of *Pasteurella* in various internal organs of flamingo carcasses arisen from a mortality event in Tanzania[38]. This is not an exhaustively comparable study but raises questions on our current understanding of the interplay between cyanobacteria and other bacteria species, including *Pasteurella*.

We do not have evidence from the ground to corroborate either *Pasteurella* spp., cyanotoxins, or a given species of cyanobacteria as the dominant cause. Our evidence shows that, at the very least, mortality was highly localised near water sources of suspect quality, from currently available remote sensing methods. Future launch of high spatial resolution sensors (order of 1-10 m) equipped with diagnostic wavebands for cyanobacteria pigment (around 620 nm), like those on current medium resolution (300 m) ocean colour sensors, would contribute greatly to diagnosing cyanobacteria dynamics in these ecosystems. Other causes, including poaching, have been previously ruled out[4], and we also show here that water was widely available in the eastern Okavango Panhandle in 2020 and death by lack of water (or drought), which can occur in elephants[39], does not seem plausible given the presence of water throughout the area at the time of the event. Factors other than cyanotoxicity might additionally have been involved, including bacterial infection, and could explain why elephants were uniquely affected and not other species also drinking from the pans. The drinking behaviour of elephants might also have played a role in their susceptibility to cyanotoxins, as drinking depth and timing might impact cyanotoxin intake due to cyanobacterial aggregation influenced by density variations, photosynthetic cycles, and environmental factors[40,41]. This can lead to different toxin concentrations at various water layers, which elephants may be more likely to encounter, especially if their drinking behaviour disturbs toxic benthic mats [42] or causes planktonic biomass to sink and accumulate at the bottom. While our research primarily focuses on planktonic cyanobacteria, these other forms could also contribute to toxicity, highlighting the complexity of these ecosystems.

The southern African region is projected to become drier and hotter[43,44], and pans across these regions will likely be subject to much shorter hydroperiods[45], with potential negative effects on water quantity and quality, and catastrophic repercussions on animals. In this context, the suggested distance covered by the elephants and the time passed after potential intoxication not only shed light on this specific event but also represents the first steps in establishing a framework for investigating future mortality events of unknown causes in large mammals. This framework could be particularly crucial in regions experiencing drastic environmental changes. More efforts to better map and characterise pan ecosystems and ecohydrology are fundamental to understanding the implications of climate change on the ecology of the Okavango and other important ecosystems in the region. We believe that the methods and findings of this study may serve future management and conservation strategies, providing a basis for addressing the challenges posed by changing environmental conditions. Integrating spatial analysis techniques in animal surveying could further serve as an early warning system to capture the onset and origin of animal mortality events, thereby offering a proactive approach to conservation. Developing a concurrent efficient sampling protocol that can be mobilised in response to or during these climatic and ecohydrological changes would add significant impact to early warning monitoring and respective management response strategies.

In conclusion, this unprecedented die-off within the largest remaining population of a threatened signature megafauna underlines the escalating concerns surrounding the impact of drought and climate change on the

Okavango Delta, one of the most important ecosystems in the world. Globally, this event underscores the alarming trend of sudden, climate-induced diseases affecting large ungulates, reflecting the broader, devastating impacts of climate change on biodiversity and ecosystem health [46,47]. By establishing a methodological approach to tracking and analysing these events, our study contributes to the broader field of environmental science and animal conservation, providing critical insights that could help mitigate similar tragedies in the future.

Methods

Study Area

Our study focused on the eastern Okavango Panhandle region, the north-easternmost sector of the Okavango Delta, which comprises the concession areas NG11, NG12 and NG13 within the Ngamiland district, Botswana. The area is enclosed to the north, east and south by a border fence and veterinary fence, originally installed to prevent the transmission of zoonotic diseases to domestic animals, like the foot and mouth disease carried by buffalos[18] and Contagious Bovine Pleuropneumonia (CBPP) [19]. The west side of the eastern Panhandle is closed-off by the Okavango River where the water is relatively deeper and prevents non-aquatic animals from routinely crossing to either side[1]. The total extent of NG11, NG12 and NG13 concession areas within the veterinary fence and including the Okavango River is around 9268km^2. The climate of Botswana is classified as arid to semi-arid, and as such it is characterised by two distinct seasons. The wet season occurs between November and March, when total rainfall range between 300mm and 600mm per year. During the dry season between April and October, rainfall is virtually absent. Temperatures average between 15ºC and 27ºC, with peak low temperatures below 0ºC at night in winter (June to August), and peak high temperatures of over 40ºC during the day in summer (November to February)[48–50]. The elephant population in Botswana is currently the largest on Earth, counting over 132,000 individuals as of the latest report from the KAZA TFCA aerial survey[51]. The most updated published record of wildlife populations within the eastern Panhandle is from a dry season survey conducted in 2018, where over 15,000 elephants were estimated, alongside 25,000 cattle, 5,000 zebras, 4,500 goats and 500 wildebeest, to mention the most abundant animals [52]. Population estimates from past and current surveys in the Panhandle, however, show large fluctuations, but the trend has shown that the population has been increasing at around 9.5% a year[53]. Reasons for such high population increases is unknown, but could be due to high immigration and low emigration from and to other areas, population structure and recruitment rates, or climatic conditions such as response to droughts,

Datasets

Data were collected and analysed with permission of the Republic of Botswana Ministry of Environment, Nature Conservation and Tourism, research permit ENT 8/36/4 XLIX (11) and Ministry of Agriculture, research permit DVS 8/2/II (28).

Elephant survey data. We used locations of elephant carcasses and live animals from an aerial survey of the eastern Okavango Panhandle conducted by the Department of Wildlife and National Parks (DWNP) of Botswana and Ecoexist[54] in July 2020 following the reported elephant mass-mortality event[20]. The aerial survey, which employed the standard methodology of strip transect sampling[55], aimed to count the number of carcasses and live animals and estimate the age category of the carcasses. The survey used the standard classification method[21] to estimate the age of the carcasses (C1 to C4, fresh carcasses to very old bones) but adjusted based on local knowledge of carcasses decay in the region. The survey classified carcasses aged <1month as fresh (C1), carcasses aged <6months as recent (C2), and those aged >6months as bones[20].

Climate data. To assess the long-term climatic conditions in the eastern Panhandle, we obtained air temperature 2 m above ground between 2015 and 2023 from the ERA5 hourly re-analysis dataset provided by the European Centre for Medium-Range Weather Forecasts (ECMWF) at a resolution of 0.25º (~25km^2)[56]. We also obtained precipitation data from the TAMSAT dataset between 2015 and 2023, which comprises rainfall estimates based on satellite and ground-based observations for the African continent at 0.0375º resolution (~4 km^2)[57–59].

Water frequency data. The location of waterholes (pans) in the eastern Panhandle, was determined using an open-source water frequency product developed for the Kavango-Zambezi Transfrontier Conservation Area (KAZA) for the period 2017-2020[60]. Sentinel-2 images and other remote sensing products were used to classify pixels within KAZA and isolate those classified as water, along with the frequency of classification.

Remote sensing data. Sentinel-2A/B Multi-Spectral Instrument Level-2A images (i.e., atmospherically, and geometrically corrected) between January 2019 and August 2023 were obtained from Google Earth Engine (GEE) using its python API. Since images prior 2019 were not available on GEE as Level-2A, individual cloud-free Sentinel-2 MSI Level-1C images between 2015 and 2018 were downloaded from CREODIAS data explorer online tool[61].

Remote sensing image processing

Sentinel-2A/B Multi-Spectral Instrument images available in GEE as Level-2A between 2019 and 2023 were filtered by cloud cover (60%) to avoid cloudy images, and pixels within each image were scanned through the *s2cloudless* algorithm[62] to mask out remaining cloud pixels and cloud shadow pixels within filtered images, discarding pixels with > 50% probability of cloud, and using the cloud shadow mask to remove likely shadow pixels. Images downloaded from CREODIAS were filtered for clouds and atmospherically corrected using the *Sen2Cor* atmospheric correction (AC) algorithm[63,64] to match the default image processing for Sentinel-2 images Level-2A by the European Space Agency (ESA).

Water frequency layer processing

Since the water frequency product contained all the pixels classified as water at least once within KAZA, we generated a custom region of interest (ROI) within the boundaries of the veterinary fence (i.e., eastern Okavango Panhandle) (Fig. 1) manually 'cropping out' the Okavango River and its north-eastern branching. The resultant ROI has an extent of 7,138 km^2. We excluded rivers and wetlands from the analysis to enhance the identification of an optimal threshold for the detection of pans, which would have been affected if perennial waters were included. The water frequency layer within the ROI was vectorised using QGIS Białowieża LTR v3.28.11, and the resultant product was a multi-polygon shapefile, where each polygon was the outline of single or group of contiguous pixels where water had been detected at least once between 2017 and 2020[60].

Identification of Pans

To identify individual pans over time, we masked the atmospherically corrected Sentinel-2 images using the vectorised water frequency product mentioned above. This allowed to exclude from the images all the pixels that fell outside individual polygons, which were assumed to be land due to the nature of the product. Since pans recede during the dry season, hence not all pixels within these polygons were expected to always have water, we identified all remaining non-water pixels within the polygons for each image using the Automated Water Extraction Index (AWEI)[17] using the equation:

$$AWEI = \rho_{B2} + 2.5 \times \rho_{B3} - 1.5 \times (\rho_{B8} + \rho_{B11}) - 0.25 \times \rho_{B12}) \quad [1]$$

where ρ_{Bn} are Sentinel-2 bands blue (B2, 490 nm), green (B3, 560 nm), NIR (B8, 705 nm), SWIR1 (B11, 1610 nm) and SWIR2 (B12, 2190 nm), respectively. This version of AWEI we adopted is also referred to as AWEI$_{sh}$. This was originally formulated to improve shadow and dark pixels areas removal in non-urban environments, pushing all non-water pixels values below 0 and pulling water pixels above 0[17]. Yet, AWEI doesn't perform in the same way across the globe, and water pixels in this part of the world show much lower values (AWEI <= -0.2)[45]. We computed an optimal AWEI threshold to mask out remaining non-water pixel from those within the polygons using the Grey Histogram method[65], which uses the distribution of the input value (here AWEI) to generate classes, minimising variance within classes and maximising variance between classes. This method determined the point at which AWEI changed due to a change in classes (i.e., water/ non-water). We calculated the optimal AWEI threshold on the 95th percentile image between Mar and May of each year, aiming to capture water at its maximum extent between the end of the wet season and the beginning of the dry season, and further exclude potential false positives (previously undetected cloud pixels), and false negative (adjacent land effects). Individual AWEI thresholds for each year were averaged to account for potential errors introduced by different light, atmospheric conditions, and computation of AC across years, obtaining a final value of -0.3624 (rounded). The threshold was applied to all the images between 2015 and 2023, and each group of contiguous pixels within each polygon was considered as an individual pan. Including the main rivers and wetlands in the formulation of the threshold would have resulted in a much higher value due to the greater number of pixels detected in much clearer waters compared to pans, which tend to have higher AWEI. Using a higher threshold would have masked out most pans in the eastern Panhandle.

To ensure continuity of measurements over time and avoid likely gaps brought by cloud filtering, masking, and/ or absence of Sentinel-2 images, we grouped all threhsolded images bi-weekly, between the 1st and the 15th, and between the 15th and the last day of each month, using the 95th percentile. This resulted in two timestamps (i.e., observations) per month. Each group of contiguous pixels within each polygon in all 95th percentile images was collated to a dataset along with the latitude and longitude of its centroid, the count of contiguous pixels, and we extracted AWEI and the Normalised Difference Chlorophyll Index (NDCI)[16] values at centroid. AWEI was used as a proxy of water availability, whereas NDCI was used as a proxy for phytoplankton biomass. NDCI was obtained using the equation:

$$NDCI = \frac{\rho_{B5} - \rho_{B4}}{\rho_{B5} + \rho_{B4}} \quad [2]$$

where ρ_{Bn} are Sentinel-2 bands near-infrared (B5, 705 nm) and red (B4, 665 nm), respectively.

Labelling pans. The final collated dataset comprised a total count of 128,667 pans between 2015 and 2023. This figure represents the aggregate count of observations, as pans were monitored multiple times (bi-weekly) during the analysis period. To discern individual water bodies, we assigned unique labels to distinguish between them based on their maximum observed extent, which was April 2021. This identification process resulted in the isolation of 3,389 distinct, or 'reference', pans from the cumulative observations. Each reference pan was defined by the centroid of its largest recorded extent and was surrounded by a 30 m radius buffer. We then matched the centroids of all recorded pan instances to these reference pan buffers at each timestamp. If a pan's centroid from any timestamp fell within this buffer, it was recognised as the same entity as the reference pan, thereby maintaining consistent identification despite potential shifts in centroid location due to changes in water levels. This methodological step ensures the accurate tracking of each unique pan over time, despite the repeated counting of the same pans across different timestamps, which initially led to the higher aggregate figure.

Location comparison between surveyed live and dead elephants

Due to the limited number of C1 carcasses points available from the 2020 aerial survey (*n=7*), C1 and C2 carcasses were combined into a single age category named *carcasses* (*n=161*). The other two categories were *bones* (*n=222*) and *live elephants* (*n=2682*). To understand if the way carcasses distributed across the eastern Panhandle differed from bones and live elephants, we computed the Nearest Neighbour Index (NNI)[66] using the equation:

$$\mathrm{NNI} = \frac{Observed\ Average\ Distance}{E[D]}; \quad [3]$$

Where:

$$E[D] = \frac{1}{2\sqrt{\lambda}};\ \lambda = \frac{n}{A}$$

Here, n is the number of points and *A* is the area of the ROI. The $Observed\ Average\ Distance$ is the average of all the distances between each pair of points. The significance of NNIs was evaluated using a Monte Carlo simulation, which randomly permuted the locations of datapoints within the ROI to simulate complete spatial randomness (CSR)[67]. The Monte Carlo simulation was set to run for 999 iterations, ensuring both statistical robustness and computational efficiency. NNI was calculated for each simulated randomly distributed set of points at each iteration and compared to the observed points using a z-score to assess the degree to which the spatial pattern of the observed points deviated from a random distribution. A z-score beyond the range of 1.96 to -1.96 indicates the presence of statistically significant clusters. The z-score was obtained with the formula:

$$\mathrm{z_{score}} = \frac{Observed\ Average\ Distance - E[D]}{\sigma_{simulated}}; \quad [4]$$

Where:

$$\sigma_{simulated} = \sqrt{\frac{\sum(x_{i,simulated} - \mu_{simulated})}{N_{simulated}}};$$

The points for each category were then crossed-compared to determine if their distributions differed statistically using the non-parametric two-sample Kolmogorov-Smirnov (KS) test, which makes use of every point in the samples irrespective of distribution and ordering[68].

Cluster identification

To further assess how carcasses, bones and live elephants distributed across the landscape, we determined the number of clusters that each category generated based on distances between points. The number of clusters in each category provided some indication on the spatial associations between points, such that fewer clusters may denote a higher likelihood of relationship between points. Clusters were determined using the DBSCAN method[69], that is a density-based algorithm that identifies within-group, distance-based clusters. DBSCAN uses an optimal average distance, referred to as *epsilon* and an arbitrary minimum number of points to generate clusters. The *epsilon* was automatically extracted from the data using an 'elbow method' algorithm, which sorted distances between points in ascending order and using a moving average identified the optimal value as the point at which distances increased sharply. The minimum number of points was set to 4 to prevent the formation of too small clusters.

Point pattern analysis

We determined which pans across the ROI elephants may have interacted with the most before dying by calculating the spatial autocorrelation between the locations of pans and the centre of each cluster for each category. Cluster centres were preferred to avoid noise brought by randomly distributed points, and to delineate areas that were common to spatially associated groups of carcasses and bones. To assess spatial autocorrelation, we used Local Moran's I[70], a statistic that we used to measure the similarity between neighbouring pans based on proximity to cluster centres. Given a set of n spatial units (i.e., the total number of pans for a given timestamp), and a variable x observed over these units (i.e., the distance between individual pans and the clusters centres), the Local Moran's I for the i^{th} unit (individual pans) is defined as:

$$I_i = \frac{n \cdot \sum_j w_{ij}(x_i - \bar{x})(x_j - \bar{x})}{2W \cdot S_0}; \quad [5]$$

Where x_i and x_j are the distances of pans i and j to the nearest cluster centre, $\bar{x}$ is the mean distance across all pans, w_{ij} is the spatial weight, indicating whether j is neighbour of pan i or not. The denominator serves as a normalisation factor, where W represent the sum of spatial weights associated with a pan, reflecting its total 'neighbouring influence' or connectivity to other pans. This is doubled to account for the reciprocal nature of spatial relationships. S_0 is the global variance of pan-cluster centres distance. The spatial weights matrix was computed applying a k-Nearest Neighbour algorithm on the locations of the pans, where the optimal *k* was dynamically calculated as the number of pans within twice the average distance between all the pans[70]. This heuristic approach ensured that the spatial weights were drawn directly from the distribution of datapoints to avoid biasing the results, which may occur when setting a fixed *k* for areas of varying point density.

Reported animal intoxication and distances covered before death

To estimate the distance that elephants may have travelled between exposure to cyanotoxins and dying, we reviewed the literature to identify the typical elephant walking speeds, and the time between exposure to cyanobacteria and death in various animals. The literature suggested that elephants in the eastern Panhandle walk an average of 4.5 km a day[22,24]. For the latter, the most relevant information were primarily extracted from the supplementary material in Wood (2016), which comprises of an extensive list of observations in published scientific literature between 1878 and 2012. In some instances, the link to cyanobacteria ingestion as cause of death was circumstantial and not proven by laboratory assessment, but with complementary empirical evidence, like observation of animal

death after interaction with water covered in green/ blue-green substance at the water surface. Only observations with relatively specific timeframe of death were used. Descriptions like 'death within days' or 'died shortly after' were discarded, since they did not provide accurate enough time estimates. Conversely, death timeframes described as 'minutes', 'few hours', or 'several hours', were kept and arbitrarily assigned to 30 minutes, 6 hours, and 12 hours, respectively.

Standard Deviation Ellipses

Standard deviation ellipses (SDE) for each carcasses clusters were computed to identify their bivariate distribution (i.e., lat-long) and statistically summarise their dispersion and orientation[23]. Since SDE are built on the distribution of the data itself, they help to identify underlying spatial trends within typical confidence intervals drawn from a normal distribution. In other words, SDE allowed to identify areas where elephants were likely to have interacted, and these 'areas of interaction' were used to further filter out pans that may have not been visited by elephants before dying. SDE was computed using the centroid of carcasses clusters and the dispersion of datapoints to determine the directionality of the ellipses. SDE was calculated using the adapted ellipse equation:

$$\frac{(x-h)^2}{(p*\sigma_x)^2} + \frac{(y-k)^2}{(p*\sigma_y)^2} = 1; \quad [6]$$

where:

$$h = \frac{1}{n}\sum_{i=1}^{n} x_i;\ k = \frac{1}{n}\sum_{i=1}^{n} y_i;$$

and

$$\sigma_x = \sqrt{\frac{1}{n}\sum_{i=1}^{n}(x_i - h)^2};\ \sigma_y = \sqrt{\frac{1}{n}\sum_{i=1}^{n}(y_i - k)^2};$$

Here, n is the total number of points, x_i and y_i are the x and y coordinates of each point, respectively, h and k are the x and y coordinates of the mean points centre, respectively. The factor p determined how many standard deviations to consider when computing the width and height of the ellipse.

References

1. Van Aarde, R. J., Pimm, S. L., Guldemond, R., Huang, R. & Maré, C. The 2020 elephant die-off in Botswana. *PeerJ* **9**, e10686 (2021).
2. Pozo, R. A., Coulson, T., McCulloch, G., Stronza, A. L. & Songhurst, A. C. Determining baselines for human-elephant conflict: A matter of time. *PLOS ONE* **12**, e0178840 (2017).
3. Maron, D. F. What's killing Botswana's elephants? Here are the top theories. https://www.nationalgeographic.com/animals/article/botswana-elephant-death-mystery (2020).
4. Azeem, S., Bengis, R., Van Aarde, R. & Bastos, A. D. S. Mass Die-Off of African Elephants in Botswana: Pathogen, Poison or a Perfect Storm? *Afr. J. Wildl. Res.* **50**, (2020).
5. Benza, B. Botswana says toxins in water killed hundreds of elephants. https://www.reuters.com/article/us-botswana-elephants-idUSKCN26C0WA/ (2020).
6. Foggin, C. M. *et al.* Pasteurella sp. associated with fatal septicaemia in six African elephants. *Nat. Commun.* **14**, 6398 (2023).
7. Huisman, J. *et al.* Cyanobacterial blooms. *Nat. Rev. Microbiol.* **16**, 471–483 (2018).
8. Paerl, H. W. & Otten, T. G. Harmful Cyanobacterial Blooms: Causes, Consequences, and Controls. *Microb. Ecol.* **65**, 995–1010 (2013).
9. Hou, X. *et al.* Global mapping reveals increase in lacustrine algal blooms over the past decade. *Nat. Geosci.* **15**, 130–134 (2022).
10. Wood, R. Acute animal and human poisonings from cyanotoxin exposure — A review of the literature. *Environ. Int.* **91**, 276–282 (2016).
11. Svirčev, Z. *et al.* Global geographical and historical overview of cyanotoxin distribution and cyanobacterial poisonings. *Arch. Toxicol.* **93**, 2429–2481 (2019).
12. Matthews, M. W., Bernard, S. & Winter, K. Remote sensing of cyanobacteria-dominant algal blooms and water quality parameters in Zeekoevlei, a small hypertrophic lake, using MERIS. *Remote Sens. Environ.* **114**, 2070–2087 (2010).
13. Dalu, T. & Wasserman, R. J. Cyanobacteria dynamics in a small tropical reservoir: Understanding spatio-temporal variability and influence of environmental variables. *Sci. Total Environ.* **643**, 835–841 (2018).
14. Bengis, R. *et al.* Eco-epidemiological and pathological features of wildlife mortality events related to cyanobacterial bio-intoxication in the Kruger National Park, South Africa. *J. S. Afr. Vet. Assoc.* **87**, (2016).
15. Veerman, J., Kumar, A. & Mishra, D. R. Exceptional landscape-wide cyanobacteria bloom in Okavango Delta, Botswana in 2020 coincided with a mass elephant die-off event. *Harmful Algae* **111**, 102145 (2022).
16. Mishra, S. & Mishra, D. R. Normalized difference chlorophyll index: A novel model for remote estimation of chlorophyll-a concentration in turbid productive waters. *Remote Sens. Environ.* **117**, 394–406 (2012).
17. Feyisa, G. L., Meilby, H., Fensholt, R. & Proud, S. R. Automated Water Extraction Index: A new technique for surface water mapping using Landsat imagery. *Remote Sens. Environ.* **140**, 23–35 (2014).
18. Perkins, J. S. 'Only connect': Restoring resilience in the Kalahari ecosystem. *J. Environ. Manage.* **249**, 109420 (2019).
19. Marobela, C. Contagious bovine pleuropneumonia in Botswana: experience with control, eradication, prevention and surveillance. *Vet Ital* **47**, (2011).
20. Songhurst, A. & Tsholofelo, C. *Elephant Population and Carcass Survey Report. Okavango Panhandle, Botswana (NG10, NG11, NG12 and NG13)*. 38 (2020).
21. Douglas-Hamilton, I. & Burrill, A. USING ELEPHANT CARCASS RATIOS TO DETERMINE POPULATION TRENDS. (1991).
22. Vogel, S. M. *et al.* Exploring movement decisions: Can Bayesian movement-state models explain crop consumption behaviour in elephants (*Loxodonta africana*)? *J. Anim. Ecol.* **89**, 1055–1068 (2020).
23. Wang, B., Shi, W. & Miao, Z. Confidence Analysis of Standard Deviational Ellipse and Its Extension into Higher Dimensional Euclidean Space. *PLOS ONE* **10**, e0118537 (2015).
24. Loarie, S. R., Aarde, R. J. V. & Pimm, S. L. Fences and artificial water affect African savannah elephant movement patterns. *Biol. Conserv.* **142**, 3086–3098 (2009).
25. African News Agency. Botswana probes mysterious death of 56 elephants. https://www.iol.co.za/news/africa/botswana-probes-mysterious-death-of-56-elephants-48239310 (2020).
26. Pozo, R. A. *et al.* Elephant space-use is not a good predictor of crop-damage. *Biol. Conserv.* **228**, 241–251 (2018).
27. Naidoo, R. *et al.* Mapping and assessing the impact of small-scale ephemeral water sources on wildlife in an African seasonal savannah. *Ecol. Appl.* **30**, (2020).
28. Songhurst, A. & Coulson, T. Exploring the effects of spatial autocorrelation when identifying key drivers of wildlife crop-raiding. *Ecol. Evol.* **4**, 582–593 (2014).
29. Songhurst, A. Measuring human–wildlife conflicts: Comparing insights from different monitoring approaches. *Wildl. Soc. Bull.* **41**, 351–361 (2017).
30. Schlossberg, S., Chase, M. J. & Sutcliffe, R. Evidence of a Growing Elephant Poaching Problem in Botswana. *Curr. Biol.* **29**, 2222-2228.e4 (2019).
31. Roever, C. L., Van Aarde, R. J. & Chase, M. J. Incorporating mortality into habitat selection to identify secure and risky habitats for savannah elephants. *Biol. Conserv.* **164**, 98–106 (2013).
32. Haynes, G. Longitudinal studies of african elephant death and bone deposits. *J. Archaeol. Sci.* **15**, 131–157 (1988).
33. Welch, E. B. & Cooke, G. D. Internal Phosphorus Loading in Shallow Lakes: Importance and Control. *Lake Reserv. Manag.* **21**, 209–217 (2005).
34. Krah, M. *et al.* Nutrient Budget in the Seasonal Wetland of the Okavango Delta, Botswana. *Wetl. Ecol. Manag.* **14**, 253–267 (2006).
35. Richer, R., Banack, S. A., Metcalf, J. S. & Cox, P. A. The persistence of cyanobacterial toxins in desert soils. *J. Arid Environ.* **112**, 134–139 (2015).
36. Cirés, S., Casero, M. & Quesada, A. Toxicity at the Edge of Life: A Review on Cyanobacterial Toxins from Extreme Environments. *Mar. Drugs* **15**, 233 (2017).
37. Chatziefthimiou, A. D., Banack, S. A. & Cox, P. A. Biocrust-Produced Cyanotoxins Are Found Vertically in the Desert Soil Profile. *Neurotox. Res.* **39**, 42–48 (2021).
38. Nonga, H. E. *et al.* Possible involvement of microcystins in the unexplained mass mortalities of Lesser Flamingo (Phoeniconaias minor Geoffroy) at Lake Manyara in Tanzania. *Hydrobiologia* **678**, 167–178 (2011).
39. Ndlovu, M. *et al.* Age-sex structure of drought-driven African elephant (Loxodonta africana) mortality in Hwange National Park, Zimbabwe. *Sci. Afr.* **19**, e01459 (2023).
40. Evans, A. M. *et al.* Nitrogen fixation by Baltic cyanobacteria is adapted to the prevailing photon flux density. *New Phytol.* **147**, 285–297 (2000).

41. Gao, Y., O'Neil, J., Stoecker, D. & Cornwell, J. Photosynthesis and nitrogen fixation during cyanobacteria blooms in an oligohaline and tidal freshwater estuary. *Aquat. Microb. Ecol.* **72**, 127–142 (2014).
42. Bouma-Gregson, K., Kudela, R. M. & Power, M. E. Widespread anatoxin-a detection in benthic cyanobacterial mats throughout a river network. *PLOS ONE* **13**, e0197669 (2018).
43. Engelbrecht, F. *et al.* Projections of rapidly rising surface temperatures over Africa under low mitigation. *Environ. Res. Lett.* **10**, 085004 (2015).
44. Nangombe, S. *et al.* Record-breaking climate extremes in Africa under stabilized 1.5 °C and 2 °C global warming scenarios. *Nat. Clim. Change* **8**, 375–380 (2018).
45. Schaffer-Smith, D. *et al.* Tracking a blue wave of ephemeral water across arid southern Africa. *Environ. Res. Lett.* **17**, 114063 (2022).
46. Kutz, S. *et al.* Erysipelothrix rhusiopathiae associated with recent widespread muskox mortalities in the Canadian Arctic. **56**, (2015).
47. Kock, R. A. *et al.* Saigas on the brink: Multidisciplinary analysis of the factors influencing mass mortality events. *Sci. Adv.* **4**, eaao2314 (2018).
48. Byakatonda, J., Parida, B. P. & Kenabatho, P. K. Relating the dynamics of climatological and hydrological droughts in semiarid Botswana. *Phys. Chem. Earth Parts ABC* **105**, 12–24 (2018).
49. Nkemelang, T., New, M. & Zaroug, M. Temperature and precipitation extremes under current, 1.5 °C and 2.0 °C global warming above pre-industrial levels over Botswana, and implications for climate change vulnerability. *Environ. Res. Lett.* **13**, 065016 (2018).
50. Akinyemi, F. O. & Abiodun, B. J. Potential impacts of global warming levels 1.5 °C and above on climate extremes in Botswana. *Clim. Change* **154**, 387–400 (2019).
51. Bussière, E. M. S. & Potgieter, D. *KAZA Elephant Survey 2022, Volume I: Results and Technical Report, KAZA TFCA Secretariat, Kasane, Botswana*. (2023).
52. Chase, M., Schlossberg, S., Sutcliffe, R. & Seonyatseng, E. DRY SEASON AERIAL SURVEY OF ELEPHANTS AND WILDLIFE IN NORTHERN BOTSWANA. (2018).
53. Songhurst, A., Chase, M. & Coulson, T. Using simulations of past and present elephant (Loxodonta africana) population numbers in the Okavango Delta Panhandle, Botswana to improve future population estimates. *Wetl. Ecol. Manag.* **23**, 583–602 (2015).
54. Ecoexist. THE ECOEXIST PROJECT: Reducing conflict and fostering coexistence between elephants and people. https://www.ecoexistproject.org (2023).
55. Norton-Griffiths, M. Counting Animals. (1978).
56. Hersbach, H. *et al.* ERA5 hourly data on single levels from 1940 to present. Copernicus Climate Change Service (C3S) Climate Data Store (CDS). https://doi.org/10.24381/cds.adbb2d47 (2023).
57. Maidment, R. I. *et al.* The 30 year TAMSAT African Rainfall Climatology And Time series (TARCAT) data set. *J. Geophys. Res. Atmospheres* **119**, (2014).
58. Tarnavsky, E. *et al.* Extension of the TAMSAT Satellite-Based Rainfall Monitoring over Africa and from 1983 to Present. *J. Appl. Meteorol. Climatol.* **53**, (2014).
59. Maidment, R. I. *et al.* A new, long-term daily satellite-based rainfall dataset for operational monitoring in Africa. *Sci. Data* **4**, 170063 (2017).
60. Swift, M., Schaffer-Smith, D. & Killea, A. Map of surface water frequency observed 2017-2020, Schaffer-Smith et al 2022. https://doi.org/10.4211/hs.6f5b34803dc247e890925d7f26b04a3b (2022).
61. CREODIAS. CREODIAS. https://explore.creodias.eu (2023).
62. Braaten, J. Sentinel-2 Cloud Masking with s2cloudless. https://developers.google.com/earth-engine/tutorials/community/sentinel-2-s2cloudless (2023).
63. ESA. *Sen2Cor Software Release Note*. http://step.esa.int/thirdparties/sen2cor/2.9.0/docs/S2-PDGS-MPC-L2A-SRN-V2.9.0.pdf (2020).
64. ESA. Sen2Cor v2.9. https://step.esa.int/main/snap-supported-plugins/sen2cor/sen2cor-v2-9/ (2020).
65. Otsu, N. A Threshold Selection Method from Gray-Level Histograms. *IEEE Trans. Syst. Man Cybern.* **9**, 62–66 (1979).
66. Diggle, P. J. *Statistical Analysis of Spatial and Spatio-Temporal Point Patterns*. (Chapman and Hall/CRC, 2013). doi:10.1201/b15326.
67. Kroese, D. P., Brereton, T., Taimre, T. & Botev, Z. I. Why the Monte Carlo method is so important today. *WIREs Comput. Stat.* **6**, 386–392 (2014).
68. Lopes, R. H. C., Reid, I. & Hobson, P. R. The two-dimensional Kolmogorov-Smirnov test. (2007).
69. Ester, M., Kriegel, H.-P. & Xu, X. A Density-Based Algorithm for Discovering Clusters in Large Spatial Databases with Noise. (1996).
70. Anselin, L. Local Indicators of Spatial Association-LISA. *Geogr. Anal.* **27**, 93–115 (1995).

Acknowledgments

We would like to thank the Government of Botswana Ministry of Environment, Nature Conservation and Tourism, Ministry of Agriculture, Department of Wildlife and National Parks, and Department of Veterinary Services for granting permission for this research to take place, as well as providing data and resources. Thank you to all the team members involved in the research. Thank you to Natural Environmental Research Council (NERC) for providing funding for this research through Urgency grant NE/V013114/1, and the London NERC DTP grant NE/S007229/1, and thank you to the Elephant Crisis Fund, DWNP and Ecoexist for co-funding the elephant population survey. For the purpose of open access, the author has applied a Creative Commons Attribution (CC BY) license to any Author Accepted Manuscript version arising.

Author contributions

D.L. designed and compiled the analysis, summarised data, produced tables and figures, interpreted the results, and drafted the original manuscript. E.J.T. designed the analysis and interpreted results. E.R.M, interpreted results and provided elephant survey. A.S and G.M collected field data and interpreted results. All authors contributed to subsequent drafts and revisions of the paper.

Competing Interest

The authors declare no competing interests.

Correspondence and request for materials should be addressed to Davide Lomeo.

Supplementary Information 1

Supplementary Figures

Supplementary Fig. 1 | Local Moran's I computed on the location of pans in April 2020. Figure showing an example for a single timestamp (15/04/2020) of the distribution of pans classified using the Local Moran's I, which is a Local Indicator of Spatial Association (LISA). The panels show the statistically significant pans (*p<0.05*) classified as close (blue) and far (red) from bones (left) and carcasses (right) cluster centres. Both bones and carcasses points are colour-coded by cluster.

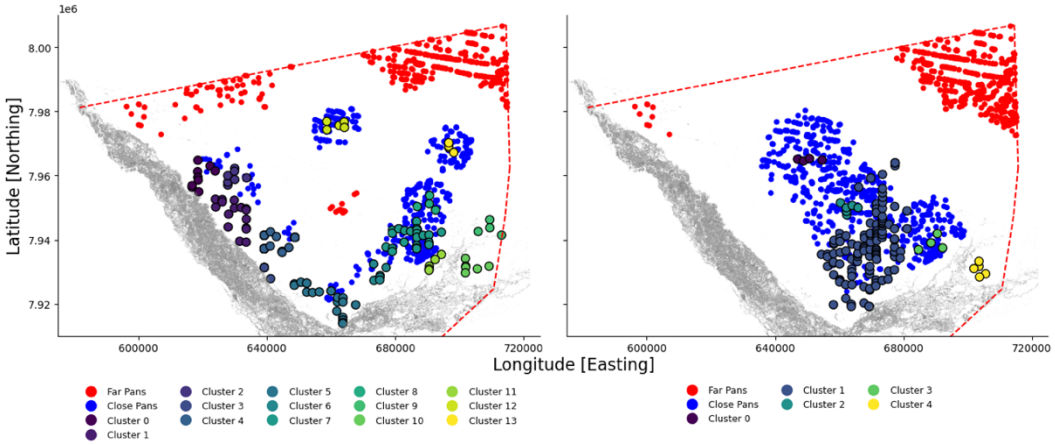

Supplementary Fig. 2 | Elephants Interaction areas and standard deviation ellipses. Figure showing how pans (blue dots), statistically associated with the location of carcasses (yellow dots), distributed in the period 2019-2020. The red, blue, and green dotted ellipses define the three standard deviations distances obtained from the spread of points along the latitude and longitude from carcass cluster centres. The circles define the potential areas of interaction after ingestion calculated using the average elephant waling speed in the area (4.5 km/ 24 hours). These were 144 hrs (or 27 km, grey circle) 120hrs (or 22.5km, cyan circle), 96 hrs (or 18 km, yellow circle), 72hrs (or 13.5km, green circle), 48hrs (or 9km, blue circle), and 24hrs (or 4.5km, red circle).

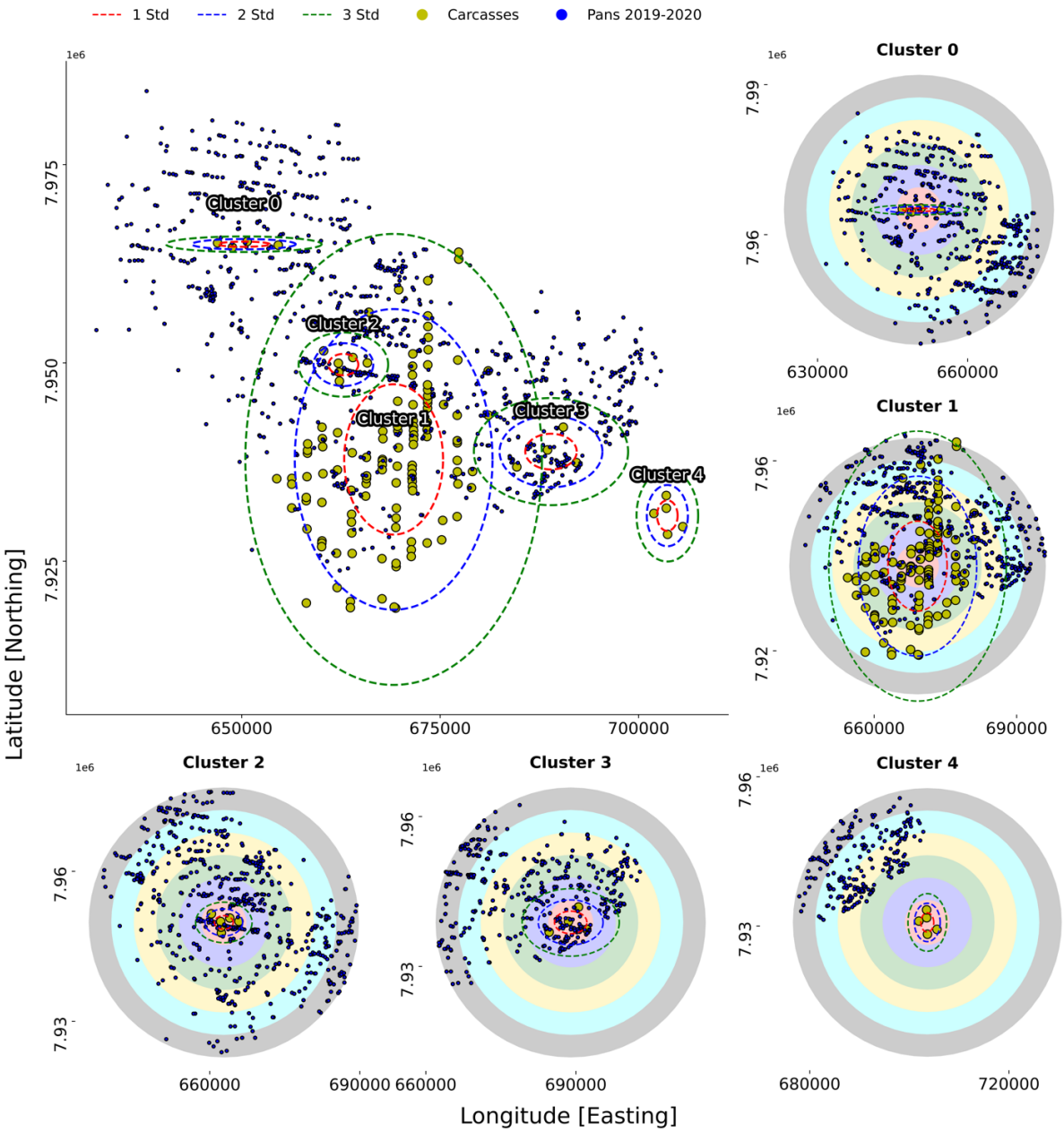

Supplementary Fig. 3 | Twenty most productive pans observed with SuperDove between April and May 2020. Figures showing true colour images of the twenty most productive pans that experienced NDCI > 0.3 and/ or an increase of NDCI of 0.1 units between consecutive timestamps at least twice in 2020. The period between April and May 2020 shown here is the period where these pans were found with the most frequent bloom events, as well as aligning with the critical period of the elephant die-off. Missing images are shown as empty white boxes. Green to bright green surface colour represent algal blooms. These can cover water surface partially or in full, depending on the severity of the bloom.

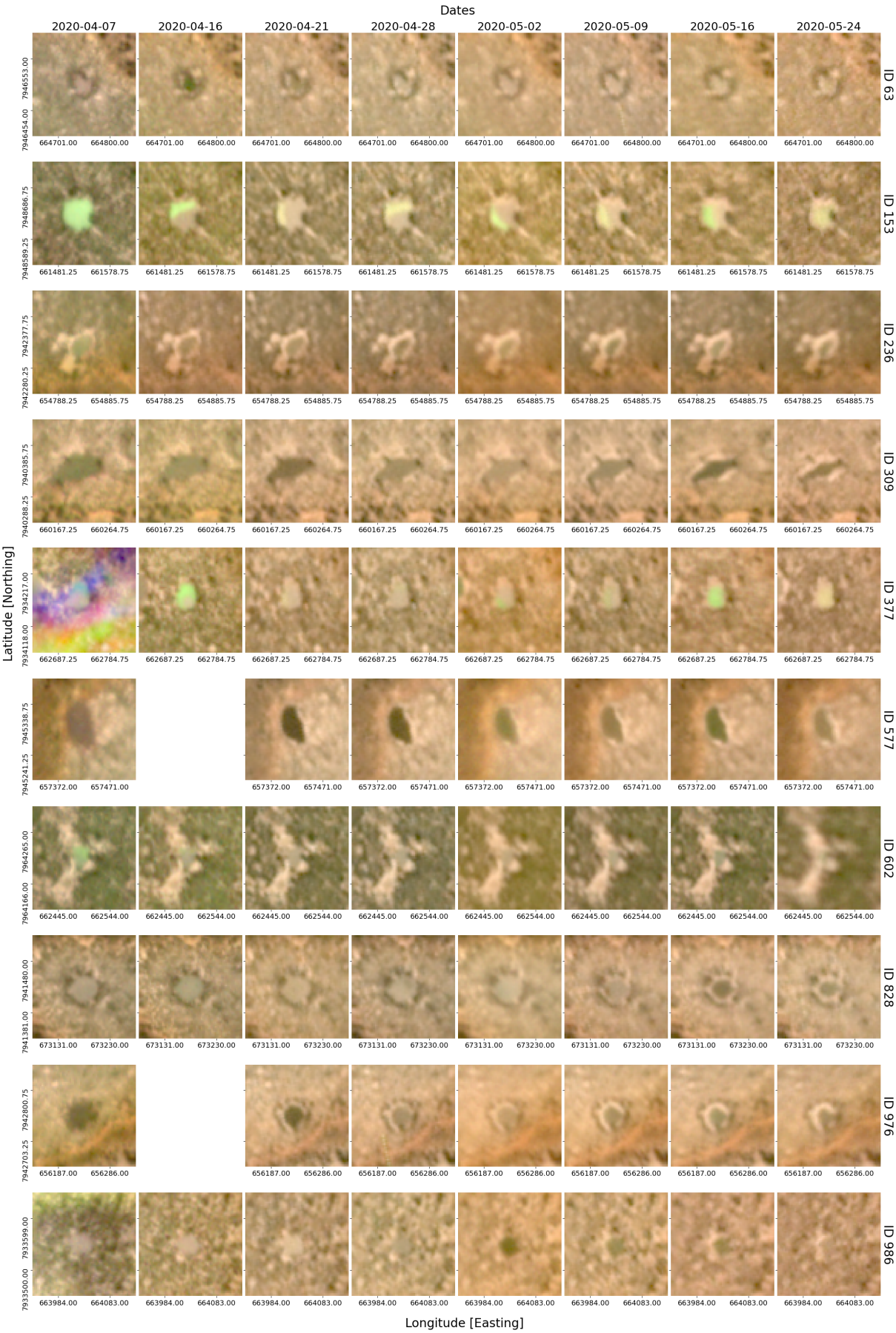
Dates
2020-04-07
2020-04-16
2020-04-21
2020-04-28
2020-05-02
2020-05-09
2020-05-16
2020-05-24
Latitude [Northing]
Longitude [Easting]
ID 63
ID 153
ID 236
ID 309
ID 377
ID 577
ID 602
ID 828
ID 976
ID 986

Supplementary Fig. 3 | *continued.*

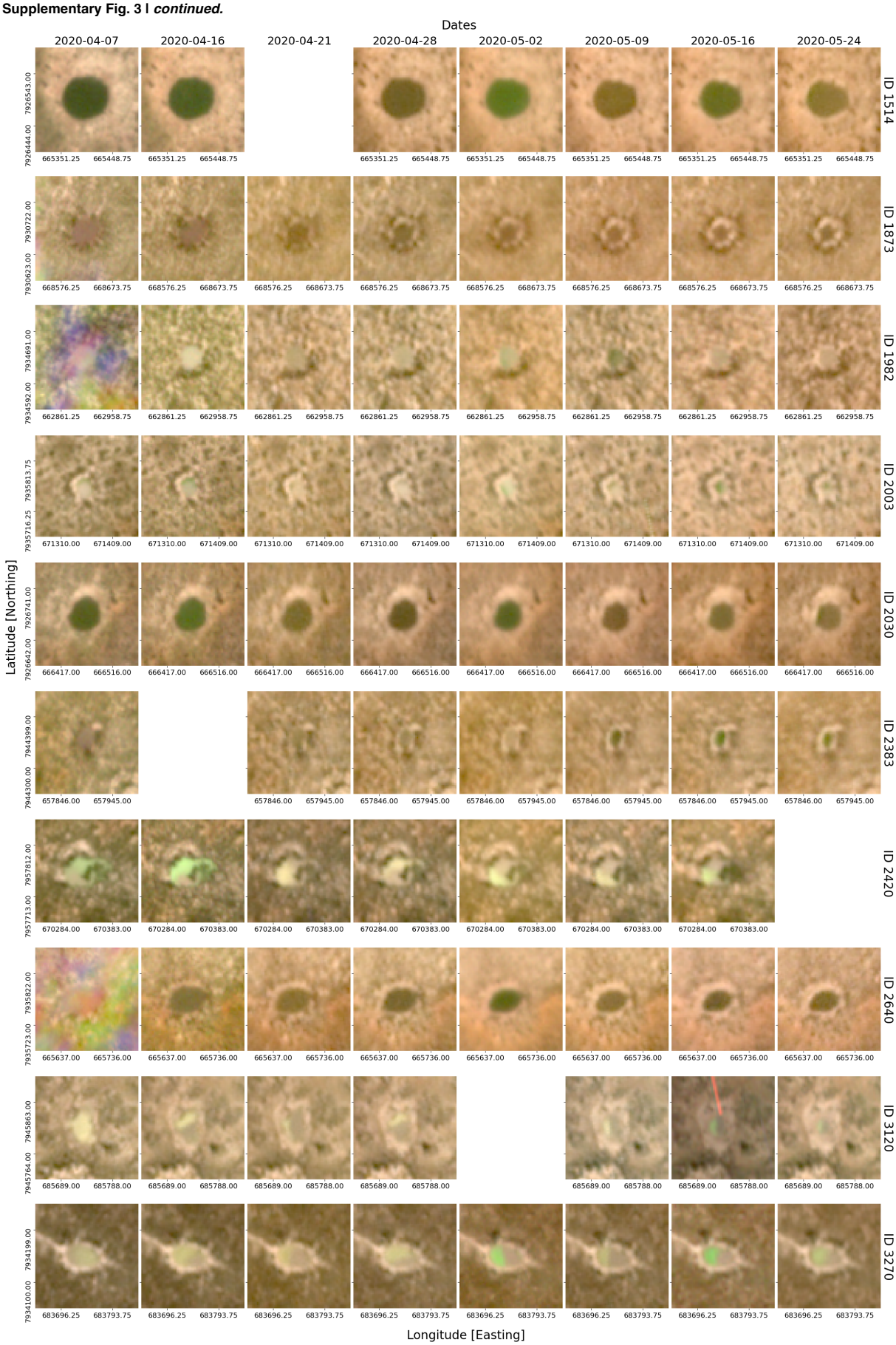

Supplementary Tables

Supplementary Table 1 l k-Nearest Neighbour Index and Two-sample T-test statistics for carcasses, bones, and live elephants.

k-Nearest Neighbour Index (NNI)			Two-samples Kolmogorov-Smirnov Test		
	NNI	**NNI (z-score)***		***p-value***	**D Statistic**
Bones	0.769	-5.947	**Bones - Carcasses**	*<0.001*	0.24
Carcasses	0.532	-10.404	**Bones - Live Elephants**	*<0.001*	0.77
Live Elephants	0.029	-92.709	**Live Elephants - Carcasses**	*<0.001*	0.83

Table showing the k-Nearest Neighbour Index (NNI) and the Two-sample Kolmogorov-Smirnov (KS) test. The NNI shows how the points for each of the categories (bones, carcasses, live elephants) distribute across the region. NNI close to 1 indicates random distribution, whereas NNI < 1 indicates clustering (higher clustering approaching 0). The NNI z-score shows the degree of clustering of each of the categories after comparison with randomly distributed points obtained with Monte Carlo simulations. The stronger the clustering, the larger the negative number. KS shows if the distributions of the coupled categories are statistically different, with D statistic indicating their similarity. D close to 0 suggest that two samples are similar, D close to 1 suggests a large difference between samples.

Supplementary Table 2 l Time in hours of death after cyanobacteria exposure for different animals.

Species	Min	Max	Mean	Observations	Cyanotoxin	Cyanobacteria	Reference
Ducks	0.50	2.00	1.25	2			
Geese	0.25	0.50	0.42	3			
Chickens	0.50	2.00	1.50	3			
Turkeys	0.50	2.00	1.00	3			
Dogs	0.25	120.00	18.49	43			
					Anatoxin-a	Anabaena sp. Lyngbya sp. Planktothrix sp. Oscillatoria sp. Phormidium favosum	Carmichael (1991) Edwards et al., (1992) Gugger *et al.,* (2005) Gunn et al., (1991, 1992) Puschner, Hoff and Tor (2008)
					Microcystin	Microcystis aeruginosa	Johnston & Jacoby (2003)
					Microcystin-LR	Anabaena sp.	Walker (2008), Backer *et al.,* (2013)
					Nodularin	Nodularia spumigena Microcystis aeruginosa	Harding (1995) Simola (2012)
Sheep	0.50	48.00	11.21	7			
Pigs	0.50	24.00	8.90	5			
Deer	1.00	4.00	2.00	1			
Horses	1.00	24.00	6.33	3			
Cattle	0.25	72.00	21.07	22			
					Cylindrospermopsin	Cylindrospermopsis raciborskii	Thomas et al. (1998) Saker, Thomas and Norton (1999) Shawn et al. (2004)
					Microcystin	Microcystis aeruginosa	Fitzgerald and Poppenga (1993)
					Microcystin-LR	Microcystis sp.	Puschner et al. (1998)
Rhinos	24.00	24.00	24.00	1			

Table showing the timeframe (in hours) of animal death after cyanobacteria exposure found in the literature. Animals are listed in order of size (top to bottom). We include a summary of cyanobacteria species and cyanotoxin reported (when both available), along with their references. Note that this information was only available for dogs and cattle.

Supplementary Table 3 | 151 most productive pans in 2020 that are spatially linked to the location of carcasses cluster centres.

Pan ID	High NDCI Count	Sharp NDCI Increase Count	Cluster	Ellipse Standard Deviation	Timeframe Cyanotoxin Ingestion-Death	Presence Jan-Jul in 2019 (%)	Presence Jan-Jul in 2020 (%)	Latitude	Longitude
496	0	1	1	1	24	21	57	-18.61411078	22.61034118
1743	1	0	1	1	48	0	64	-18.72451833	22.59481645
1719	1	2	1	1	48	0	57	-18.60867169	22.64824153
1371	0	1	1	1	48	7	64	-18.66746643	22.54807937
1297	0	2	1	1	48	14	57	-18.69915129	22.55948156
1177	0	1	1	1	48	0	50	-18.706769	22.63673668
1144	0	3	1	1	24	14	57	-18.6638475	22.62694504
2407	0	1	1	1	24	35	57	-18.61496632	22.60607846
2797	1	0	1	1	48	0	78	-18.68335319	22.55252778
2640	0	3	1	1	24	14	71	-18.66267969	22.57086771
828	2	2	1	1	48	7	57	-18.61092637	22.6414632
839	0	2	1	1	24	14	64	-18.6416142	22.56408543
2716	0	1	1	1	24	21	57	-18.61640362	22.62521578
2669	0	1	1	1	24	7	50	-18.64489305	22.59936676
2689	0	2	1	1	48	0	57	-18.63264843	22.54609449
986	2	2	1	1	48	7	71	-18.68286612	22.55543914
3196	1	1	1	1	24	42	57	-18.66211141	22.56671007
2144	1	2	1	1	48	0	64	-18.68265822	22.63247866
1873	2	1	1	1	48	0	57	-18.70849377	22.59920956
1931	0	1	1	1	48	14	42	-18.70695915	22.63833867
1904	1	3	1	1	48	35	92	-18.60216532	22.55477824
70	1	1	1	1	48	7	21	-18.70003164	22.59160532
134	0	2	1	1	48	35	50	-18.62011107	22.55374328
2003	2	1	1	1	24	7	50	-18.66225748	22.62469027
2383	2	0	1	2	72	14	64	-18.5857594	22.4963892
1982	3	2	1	2	48	0	57	-18.67308518	22.54470128
1031	0	1	1	2	48	0	71	-18.65858038	22.53184938
1019	0	1	1	2	72	0	57	-18.57109645	22.65061565
1010	0	1	1	2	72	21	57	-18.54172653	22.54296753
969	0	1	1	2	72	7	28	-18.54814449	22.55874794
2011	1	1	1	2	72	28	71	-18.54535223	22.55999061
2030	3	2	1	2	72	7	71	-18.74462933	22.57907482
2220	0	1	1	2	96	7	57	-18.53593406	22.51807422
2181	0	1	1	2	96	0	35	-18.51138842	22.66738919
2616	0	1	1	2	96	7	64	-18.48550262	22.61847842
1038	0	1	1	2	72	0	35	-18.52662984	22.56913845
1978	0	1	1	2	72	0	28	-18.56260921	22.62697339
1830	0	1	1	2	96	7	42	-18.5188145	22.6330985
2233	0	1	1	2	72	35	85	-18.54432434	22.57443788
1185	1	1	1	2	72	7	28	-18.65408281	22.69751669
1924	1	0	1	2	72	35	85	-18.55129758	22.60223239
1399	0	1	1	2	72	50	85	-18.54487912	22.5560747
1417	0	1	1	2	48	0	64	-18.67763664	22.54209916
1514	3	2	1	2	72	14	78	-18.74650645	22.56898512
1520	0	1	1	2	48	0	50	-18.67530289	22.53747658
945	1	0	1	2	96	14	57	-18.51266104	22.53911675
1530	0	1	1	2	96	0	50	-18.50259092	22.61954292
2326	0	2	1	2	96	7	50	-18.54468598	22.50809793
1780	0	1	1	2	96	0	50	-18.53383433	22.52001857
2417	1	0	1	2	72	21	85	-18.55244143	22.60578223
1040	1	2	1	2	72	21	78	-18.68672759	22.69062661
26	0	1	1	2	48	0	78	-18.6716853	22.53655206
922	0	1	1	2	72	35	64	-18.54873328	22.55087238
2699	1	0	1	2	72	14	64	-18.63824551	22.48712227
886	0	1	1	2	96	7	64	-18.52361012	22.5482388
471	1	1	1	2	72	14	64	-18.5824781	22.49668034
431	1	1	1	2	72	0	35	-18.55317506	22.60448716
377	2	2	1	2	48	0	64	-18.6773864	22.54308731
3167	0	1	1	2	72	21	57	-18.56161922	22.54097423
3200	1	1	1	2	72	57	64	-18.56675595	22.55539014
319	0	1	1	2	72	0	35	-18.72415141	22.55691238
309	0	2	1	2	72	21	71	-18.62186333	22.51857972
294	0	1	1	2	72	7	21	-18.56688819	22.66452917
264	0	1	1	2	96	0	78	-18.49604221	22.61313344
3257	0	1	1	2	48	0	50	-18.66218562	22.53331813
3278	0	1	1	2	96	7	42	-18.48488385	22.60579613
153	2	2	1	2	72	35	85	-18.54673458	22.53048844
63	2	2	1	2	72	28	50	-18.56577034	22.56117309
46	0	1	1	2	72	35	64	-18.54586415	22.56526015
42	1	1	1	2	72	28	85	-18.55175949	22.60016728
35	1	1	1	2	48	0	35	-18.65967033	22.68677284
3090	1	1	1	2	96	7	71	-18.48660989	22.60163501
560	0	1	1	2	48	0	50	-18.61250878	22.66332681
3125	0	1	1	2	48	21	57	-18.58874834	22.55207046
2175	0	1	1	2	96	7	28	-18.48521751	22.58557762
762	1	0	1	2	96	0	50	-18.5109637	22.66102547
2752	0	1	1	2	72	50	85	-18.54894071	22.60742989
737	0	2	1	2	96	7	57	-18.55727736	22.70169984
2775	0	1	1	2	72	42	85	-18.54656967	22.57226256
585	1	0	1	2	96	14	78	-18.4859137	22.62689149
701	0	1	1	2	48	0	35	-18.664117	22.6769812
627	1	0	1	2	72	21	64	-18.56347873	22.64879207
572	1	1	1	2	96	7	21	-18.49415574	22.57987332
2757	0	1	1	3	144	0	28	-18.42453223	22.58842161
2796	1	3	1	3	96	7	78	-18.56719741	22.71100144
3270	2	2	1	3	96	0	71	-18.67578948	22.74223258
3232	1	0	1	3	120	35	92	-18.55961949	22.457058
2830	0	1	1	3	120	0	57	-18.68599097	22.77135421
2310	0	2	1	3	144	0	50	-18.42588378	22.59496502

3213	0	1	1	3	120	14	78	-18.4662406	22.53725949
2464	1	1	1	3	120	21	35	-18.66883579	22.7731551
2582	0	1	1	3	96	0	57	-18.59265601	22.44622646
3029	0	1	1	3	120	7	42	-18.50583384	22.47542988
3037	0	1	1	3	120	7	71	-18.46088215	22.61631797
3139	0	1	1	3	120	7	50	-18.45604644	22.52656867
2526	1	0	1	3	144	7	21	-18.42821532	22.60164521
2419	0	1	1	3	120	0	28	-18.68238447	22.77858584
2420	4	3	1	3	120	28	92	-18.46359408	22.61310102
2492	1	2	1	3	120	7	21	-18.45781889	22.58171486
3120	2	1	1	3	120	7	50	-18.57024305	22.76003757
3045	1	1	1	3	120	7	57	-18.54725146	22.44172432
2451	0	1	1	3	96	42	78	-18.61702231	22.75181962
2932	0	1	1	3	120	0	42	-18.46406382	22.64653215
2605	0	1	1	3	144	0	35	-18.4384602	22.51589081
1513	0	1	1	3	120	0	42	-18.46118757	22.59581841
2093	0	1	1	3	120	7	50	-18.47037285	22.49370991
711	0	1	1	3	96	0	21	-18.62831659	22.76617162
708	0	2	1	3	120	14	64	-18.45763923	22.55047595
650	0	1	1	3	120	21	64	-18.64421931	22.77678403
636	0	1	1	3	96	7	50	-18.63054633	22.7633364
632	0	1	1	3	96	7	57	-18.56000225	22.45812914
602	2	1	1	3	n/a	28	50	-18.40590852	22.53837115
577	0	4	1	3	96	21	85	-18.57732412	22.49179643
531	1	1	1	3	96	0	35	-18.64447982	22.74559452
512	1	1	1	3	96	0	64	-18.69577063	22.72466228
486	1	0	1	3	120	0	78	-18.57843602	22.43600896
417	0	1	1	3	96	7	42	-18.61969058	22.44836469
363	0	1	1	3	120	14	14	-18.5235576	22.72653227
362	0	1	1	3	120	0	57	-18.54270581	22.444213
341	0	2	1	3	96	21	64	-18.52978143	22.49454085
284	0	1	1	3	96	0	57	-18.57168035	22.73478779
236	3	2	1	3	96	0	50	-18.6042394	22.46757512
218	0	1	1	3	120	7	35	-18.68156164	22.77211086
206	1	1	1	3	120	21	92	-18.48708103	22.51061178
205	0	1	1	3	96	7	64	-18.64273709	22.74574724
726	0	1	1	3	120	0	35	-18.52825429	22.73560002
738	1	1	1	3	96	0	71	-18.68058611	22.75166114
749	0	1	1	3	144	7	14	-18.43201928	22.5051245
840	0	1	1	3	144	28	92	-18.43658919	22.53081974
2077	0	2	1	3	144	0	42	-18.42888316	22.59102241
1965	0	1	1	3	120	14	50	-18.52308608	22.73588181
1905	0	1	1	3	72	14	64	-18.60931976	22.72611905
1882	1	1	1	3	96	0	28	-18.64610577	22.74417518
1851	0	1	1	3	96	0	35	-18.67676527	22.7398992
1823	0	1	1	3	120	0	14	-18.57284816	22.76052452
1812	0	1	1	3	120	0	42	-18.48454377	22.50456883
1644	1	1	1	3	144	7	42	-18.44024784	22.6086763
1595	0	1	1	3	144	0	50	-18.42376685	22.58688128
2177	0	1	1	3	144	7	50	-18.44551197	22.49049095
3327	0	1	1	3	144	0	28	-18.43962801	22.51555394
1362	0	1	1	3	120	14	35	-18.51845517	22.75585328
1295	0	1	1	3	144	7	57	-18.43709476	22.6147549
1126	0	1	1	3	120	0	57	-18.47641402	22.55618025
1046	0	1	1	3	96	0	35	-18.61770404	22.44294512
1037	0	1	1	3	120	0	64	-18.57826051	22.43755514
976	0	2	1	3	96	21	57	-18.60033661	22.48078914
948	0	2	1	3	120	28	85	-18.45828251	22.56539103
869	0	1	1	3	120	0	28	-18.67891829	22.77412858
857	1	0	1	3	120	14	85	-18.5519389	22.44102209
1390	0	2	1	3	120	7	42	-18.56946825	22.76390443
3376	0	1	1	3	144	14	50	-18.42198836	22.5818149

Table of individually labelled pans with relative coordinates that have showed either NDCI >= 0.3 (High NDCI Count), or a sharp increase of NDCI of 0.1 units between consecutive timestamps (Sharp NDCI Increase Count') in 2020 within the three standard deviation ellipses from carcass cluster centre 1. Cluster refers to the carcass cluster each pan was spatially related to. The 'Presence' columns show how often, on a bi-weekly average, each pan saw water in the period Jan-Jul 2019 and 2020.

References in Supplementary Information

Backer, LC, Landsberg, JH, Miller, M, Keel, K & Taylor, TK 2013, 'Canine cyanotoxin poisonings in the United States (1920s–2012): Review of suspected and confirmed cases from three data sources', *Toxins*, vol. 5, no. 9, pp. 1597-1628.

Carmichael, WW 1991, 'Blue-green algae: An overlooked health threat', *Health & Environment Digest*, vol. 5, no. 6, pp. 1-4.

Edwards, C, Beattie, KA, Scrimgeour, CM & Codd, GA 1992, 'Identification of anatoxin-a in benthic cyanobacteria (blue-green algae) and in associated dog poisonings at Loch Insh, Scotland', *Toxicon*, vol. 30, no. 10, pp. 1165-1175.

Fitzgerald, SD & Poppenga, RH 1993, 'Toxicosis due to microcystin hepatotoxins in three Holstein heifers', *Journal of Veterinary Diagnostic Investigation*, vol. 5, no. 4, pp. 651-653.

Gugger, M, Lenoir, S, Berger, C, Ledreux, A, Druart, J-C, Humbert, J-F, Guette, C & Bernard, C 2005, 'First report in a river in France of the benthic cyanobacterium *Phormidium favosum* producing anatoxin-a associated with dog neurotoxicosis', *Toxicon*, vol. 45, no. 7, pp. 919-928.

Gunn, GJ, Rafferty, AG, Rafferty, GC, Cockburn, N, Edwards, C, Beattie, KA & Codd, GA 1992, 'Fatal canine neurotoxicosis attributed to blue-green algae (cyanobacteria)', *The Veterinary Record*, vol. 130, no. 14, pp. 301-302.

Gunn, GJ, Raffery, AG, Rafferty, GC, Cockburn, N, Edwards, C, Beattie, KA & Codd, GA 1991, 'Additional algal toxicosis hazard', *The Veterinary Record*, vol. 129, p. 391.

Harding, WR, Rowe, N, Wessels, JC, Beattie, KA & Codd, GA 1995, 'Death of a dog attributed to the cyanobacterial (blue-green algal) hepatotoxin nodularin in South Africa', *Journal of the South African Veterinary Association*, vol. 66, no. 4, pp. 256-259.

Johnston, BR & Jacoby, JM 2003, 'Cyanobacterial toxicity and migration in a mesotrophic lake in western Washington, USA', *Hydrobiologia*, vol. 495, no. 1-3, pp. 79-91.

Puschner, B, Hoff, B & Tor, ER 2008, 'Diagnosis of anatoxin-a poisoning in dogs from North America', *Journal of Veterinary Diagnostic Investigation*, vol. 20, no. 1, pp. 89-92.

Saker, ML, Thomas, AD & Norton, JH 1999, 'Cattle mortality attributed to the toxic cyanobacterium *Cylindrospermopsis raciborskii* in an outback region of North Queensland', *Environmental Toxicology*, vol. 14, no. 1, pp. 179-182.

Shaw, GR, McKenzie, RA, Wickramasinghe, WA, Seawright, AA, Eaglesham, GK & Moore, MR 2004, *Comparative toxicity of the cyanobacterial toxin cylindrospermopsin between mice and cattle: human implications*, Florida Fish and Wildlife Conservation Commission, Florida Institute of Oceanography, and Intergovernmental Oceanographic Commission of UNESCO.

Simola, O, Wiberg, M, Jokela, J, Wahlsten, M, Sivonen, K & Syrjä, P 2012, 'Pathologic findings and toxin identification in cyanobacterial (*Nodularia spumigena*) intoxication in a dog', *Veterinary Pathology*, vol. 49, no. 5, pp. 755-759.

Thomas, AD, Saker, ML, Norton, JH & Olsen, RD 1998, 'Cyanobacterium *Cylindrospermopsis raciborskii* as a probable cause of death in cattle in northern Queensland', *Australian Veterinary Journal*, vol. 76, no. 9, pp. 592-594.

Walker, SR, Lund, JC, Schumacher, DG, Brakhage, PA, McManus, BC, Miller, JD, Augustine, MM, Carney, JJ, Holland, RS & Hoagland, KD 2008, 'Nebraska experience', in *Cyanobacterial Harmful Algal Blooms: State of the Science and Research Needs*, ed. HK Hudnell, Springer, pp. 139-152.